

Mathematical modelling of hypoglycaemia and lactic acidosis
in the bloodstream of *Plasmodium berghei* infected rats: a
feasibility study

by

Nicolas Walters



*Thesis presented in partial fulfilment of the requirements for the degree
of Master of Science in Biochemistry in the Department of
Biochemistry at Stellenbosch University*

Supervisor: Prof. J.L. Snoep

2016

Declaration

By submitting this thesis electronically, I declare that the entirety of the work contained therein is my own, original work, that I am the sole author thereof (save to the extent explicitly otherwise stated), that reproduction and publication thereof by Stellenbosch University will not infringe any third party rights and that I have not previously in its entirety or in part submitted it for obtaining any qualification.

Date:March 2016.....

Copyright © 2016 Stellenbosch University
All rights reserved.

Abstract

Mathematical modelling of hypoglycaemia and lactic acidosis in the bloodstream of *Plasmodium berghei* infected rats: a feasibility study

N. Walters

*Department of Biochemistry,
University of Stellenbosch,
Private Bag X1, 7602 Matieland, South Africa.*

Thesis: MSc (Biochemistry)

2016

Needless prescription and overuse of anti-microbial compounds served as a catalyst for the evolution and rise of multiple drug resistant pathogens, one of humanities greatest threats in the anti-biotic era. Resistance to our last line of defence drugs for malaria, a disease that reportedly caused the deaths of more than half a million people in 2013, is being reported in South-east Asia, necessitating the need for a novel high throughput method of anti-malarial drug development. Advances in the field of systems biology and further development of metabolic control analysis, could be used to identify drug targets from metabolic models.

The purpose of this project was to investigate the feasibility of creating a whole body model of rats infected with *P. berghei*. To assess the feasibility, a initiatory glycolytic model was constructed and the possibility of modelling the change in blood parameters over the course of a malarial infection was investigated. Wistar rats were infecting with *P. berghei*, ANKA strain, and blood parameters, including blood glucose and lactate concentration, haematocrit and parasitemia was measured and the relationship between the parameters evaluated. Furthermore, pulse experiments were performed to analyse the possibility of modelling the homeostatic potential of the rat. Microscopy and enzymatic glucose and lactate concentration determinations proved to be reliable and accurate methods to measure blood parameters. In addition, a relationship between parasitemia and the other blood parameters could be quantified, providing evidence that the physiological changes during malarial infection could be modelled. The glycolytic enzymes were liberated from the parasites and biochemically characterized. The kinetic parameters obtained from the characterization were subsequently used to construct a glycolytic model. Steady state concentrations predicted by the preliminary model fall within physiological ranges,

indicating that the model construction is feasible.

In conclusion, the results from the experiments, biochemical characterization of the glycolytic enzymes isolated from *P. berghei* and preliminary model construction of the glycolytic pathway supports the feasibility of creating a complete whole body model, warranting further investigation.

Acknowledgement

I would like to express my deepest gratitude to the following people for making this project possible and helping me on my voyage to complete it:

Prof Jacky Snoep for giving me this great opportunity to take on this project, the unselfish funding and the insightful guidance throughout.

Prof Lubbe Wiesner, Dr. Liezl Gibhard and Mr. Trevor Finch from Clinical pharmacology at Grootte Schuur Hospital, South Africa, for selflessly assisting me with the rat section of the project.

Arrie Arends, whose incredible organisational skills made working in the lab remarkably more efficient and trouble-free.

My peers in the molecular and systems biology lab who never shied away from assisting with experiments or engaging in friendly banter.

Sean O’Kennedy, Trevor Richie and Sasha-Lee Maggs who abandoned other obligations to assist a friend in the gloomy hours of the night.

The NRF for feeding a hungry student with a generous bursary, enabling me to complete my work without the troubles of financial stability.

Contents

Declaration	2
Abstract	3
Contents	6
List of Figures	8
List of Tables	9
1 General Introduction	12
2 Rat blood analysis	16
2.1 Introduction	16
2.2 Methods and Materials	19
2.2.1 Materials	19
2.2.2 Ethical Clearance	19
2.2.3 Inoculation and acquisition of the rats	19
2.2.4 Daily blood sampling	19
2.2.5 Determining parasitemia with microscopy	19
2.2.6 Determining haematocrit with microscopy	21
2.2.7 Blood glucose concentration determination	21
2.2.8 Blood lactate concentration determination	21
2.2.9 Pulse experiments	21
2.2.10 Computational analysis and statistics	22
2.3 Results and Discussion	22
2.3.1 Parasitemia	22
2.3.2 Haematocrit	22
2.3.3 Blood glucose and lactate	23
2.3.4 Pulse Results	25
2.3.5 Summary	28
3 Enzymes kinetics	29
3.1 Introduction	29
3.1.1 Kinetic parameter quantification	30
3.1.2 Glycolytic enzymes	31
3.2 Methods and Materials	35

3.2.1	Materials	35
3.2.2	Isolation of intact Parasites	35
3.2.3	Protein concentration determination	36
3.2.4	Characterizing glycolytic enzymes	36
3.2.5	Computational Analysis and Statistics	39
3.3	Results and Discussion	39
3.3.1	Hexokinase	39
3.3.2	Glucosephosphate isomerase	40
3.3.3	Phosphofructokinase	42
3.3.4	Aldolase	43
3.3.5	Triosephosphate isomerase	43
3.3.6	Glyceraldehyde 3-phosphate dehydrogenase	44
3.3.7	Phosphoglycerate kinase	46
3.3.8	Phosphoglycerate mutase	48
3.3.9	Enolase	48
3.3.10	Pyruvate kinase	50
3.3.11	Lactate dehydrogenase	52
3.3.12	Summary	52
4	Model construction	57
4.1	Introduction	57
4.2	Methods	58
4.2.1	Mathematical modeling	58
4.2.2	Constraints, assumptions and conserved moieties	58
4.2.3	Model analysis	59
4.3	Results and Discussion	62
4.3.1	Summary	63
5	General discussion, future work and conclusion	66
A	Buffers and Media Composition	69
B	Full Rat Blood Analysis Data	71
C	Full model fluxes	73
	List of References	76

List of Figures

1.1	Diagram of <i>Plasmodium</i> life cycle	13
2.1	Simplified schematic of influences on blood glucose and lactate	17
2.2	Experimental design	20
2.3	Results from the parasitemia measured per day post inoculation	23
2.4	Blood slides of a rat over the course of the infection	24
2.5	Results from the haematocrit measurements over the course of the infection	25
2.6	Blood glucose and lactate concentrations over the course of the infection	26
2.7	Blood glucose and lactate concentration from the pulse experiments . . .	27
3.1	Glycolysis	32
3.2	Hexokinase	40
3.3	Glucosephosphate isomerase	42
3.4	Phosphofructokinase	44
3.5	Aldolase	45
3.6	Triosephosphate isomerase	46
3.7	Glyceraldehyde 3-phosphate dehydrogenase	47
3.8	Phosphoglycerate kinase	49
3.9	Phosphoglycerate mutase	50
3.10	Enolase	51
3.11	Pyruvate kinase	53
3.12	Lactate dehydrogenase	55
4.1	Metabolite concentrations for model over time course from JWS Online and steady state concentrations	62
4.2	A heat map created by JWS online that shows the difference in relative flux control the different enzymes have on the glycolytic model	63
4.3	Metabolite concentrations for the corrected model over time course from JWS Online and steady state concentrations	64
B.1	Full parasitemia	71
B.2	Full Haematocrit	71
B.3	Full Blood Glucose and lactate	72
B.4	Full Blood Average Glucose and lactate	72
C.-1	Metabolite concentrations of the model over time from Mathematica 10.0	75

List of Tables

3.1	Hexokinase	41
3.2	Glucosephosphate isomerae	41
3.3	Phosphofructokinase	43
3.4	Aldolase	45
3.5	Triosephosphate isomerase	46
3.6	Glyceraldehyde 3-phosphate dehydrogenase	47
3.7	Phosphoglycerate kinase	48
3.8	Phosphoglycerate mutase	50
3.9	Enolase	51
3.10	Pyruvate kinase	52
3.11	Lactate dehydrogenase	54
3.12	Summary of kinetic data from the enzyme characterization	56
4.1	Starting metabolite concentrations for creation of the model	59
4.2	Model steady state metabolites concentrations	64
4.3	Model steady state enzyme flux	65
A.1	Enzyme Assay Buffer	69
A.2	Culture Media	69
A.3	Glu-Lac-Determination Buffer	70
A.4	CPDA	70

Abbreviations

α -GlyPDH	α -glycerophosphate dehydrogenase
2PG	2-phosphoglycerate
3PG	3-phosphoglycerate
Acetyl-CoA	acetyl-coenzyme A
ADP	adenosine diphosphate
ALD	fructose biphosphate aldolase
ALD	aldolase
ATP	adenosine triphosphate
B13PG	1,3-bisphosphoglycerate
DHAP	dihydroxyacetone phosphate
ENO	enolase
F16BP	fructose-1,6-bisphosphate
F6P	fructose-6-phosphate
G6P	glucose-6-phosphate
G6PDH	glucose-6-phosphate dehydrogenase
GAP	glyceraldehyde-3-phosphate
GAPDH	glyceraldehyde-3-phosphate Dehydrogenase
Glu	glucose
GPI	glucosephosphate isomerase
HEPES	4-(2-hydroxyethyl)piperazine-1-ethanesulfonate
HK	hexokinase
K_m	Michaelis constant
kDa	kiloDalton
Lac	lactate
LDH	lactate dehydrogenase
mRNA	message ribonucleic acid
MCA	metabolic control analysis
NAD^+	nicotinamide adenine dinucleotide
NADH	nicotinamide adenine dinucleotide, reduced
$NADP^+$	nicotinamide dinucleotide phosphate
NADPH	nicotinamide dinucleotide phosphate, reduced
PEP	phosphoenol pyruvate
PFK	phosphofruktokinase
PGK	phosphoglycerate kinase
PGM	phosphoglycerate mutase
Pi	inorganic phosphate

PK	pyruvate Kinase
Pyr	pyruvate
RBC	red blood cell
TPI	triosephosphate isomerase

Chapter 1

General Introduction

One of humanities greatest obstacles of the 21st century is countering the emerging multidrug-resistant diseases. The overuse and needless prescription of antibiotics and other anti-microbial medicament served as a catalyst for the evolution of the multiple-drug resistant organisms. Multiple-drug resistant *Mycobacterium tuberculosis* is of great concern, especially in third world countries where reliable medicine is hard to come by (Johnston *et al.*, 2009). *Staphylococcus aureus*, another infectious pathogen, is rapidly gaining resistance to all anti-biotic classes, is becoming increasingly difficult to treat (Enright *et al.*, 2002). Immunocompromised patients, those with AIDS (acquired immune deficiency syndrome) and other immunocompromising diseases, are particularly susceptible to multiple-drug resistant *S. aureus* as it is a opportunistic infections, most commonly found in hospitals (Archer, 1998).

According to the latest estimates of the World Health Organisation (WHO) released in December 2014, 584 000 deaths were caused by malaria infection in the year 2013. Children are the most vulnerable to malaria and it is estimated that a child dies every minute of malaria, predominantly in Africa (WHO, World Malaria Report 2014). Malaria has plagued humans for millennia, but humans managed to drive the disease to mainly equatorial countries with the discovery and use of quinine (Peters *et al.*, 1970). First reports of quinine resistance appeared in 1910 and humans were forced to find a new anti-malarial drug and as a result, chloroquine, the famous antimalarial drug, was discovered at Elberfeld Laboratories in 1934 (Coatney *et al.*, 1963). During the 1980's, chloroquine resistance malaria arose across Africa, Southeast Asia and South America, forcing, yet again, the drive for novel drug development (Wernsdorfer and Payne, 1991). Sulfadoxine-pyrimethamine, a cost-effective and efficient antimalarial drug discovered by Guttman and Ehrlich (Carson, 1984), and mefloquine was discovered soon after and allocated as the first-line of defence drugs for malarial treatment, but resistance to these drugs is present today (Wongsrichanalai *et al.*, 2002) (Miller and Su, 2011). Recent advancements by the researchers at the University of Cape Town led to the discovery of a unique antimalarial, 2-Aminopyridine MMV390048, drug which is still in pre-clinical trails (Younis *et al.*, 2014), but shows promise. History clearly tells a grim tale of the rate of drug discovery being significantly slower than drug resistance evolution and a new high throughput antimalarial drug development method is needed as the resistance to our last-line-of-defence drug, the costly artemisinin, is being reported in

Southeast Asia (WHO, World Malaria Report 2014).

Malarial infection has four conserved and distinct phases across all the different *Plasmodium* species. An overview of the life-cycle is displayed in figure 1.1. The gametocytes, the sexual forms of the parasite, fertilise in the midgut lumen of a female *Anopheles* mosquito, producing zygotes that develop into motile ookinetes, altering the status of the mosquito from non-communicable to infectious (Dimopoulos *et al.*, 1998). The motile ookinetes develop into oocysts and rupture, releasing motile sporozoites, which infects the salivary glands. During a blood meal, the sporozoites are injected into the bloodstream of the animal the mosquito is feeding on and, by travelling through the bloodstream, reaches the liver and subsequently infects the hepatocytes (Amino *et al.*, 2006). The intracellular sporozoites differentiate to form merozoites, which are released directly into the blood stream to start the asexual phase, also known as the blood stage, of the malarial life cycle (Sturm *et al.*, 2006). During the asexual phase, the merozoites invade red blood cells (RBCs), also known as a erythrocyte, to replicate. *Plasmodium berghei*, the primary focus of this study, selectively invades young reticulocytes (affinity 150-fold greater compared to mature RBCs), complicating growing the organism *in vitro* (Cromer *et al.*, 2006). During the blood stage, the parasites consumes nutrients through the parasitophorous vacuole membrane by means of highly efficient transporters as well as metabolising the haemoglobin molecules within a vacuolar compartment known as a digestive vacuole, excreting toxic heme crystals as detoxified hemozoin in return (Wunderlich *et al.*, 2012). The merozoites develop into rings, trophozoites, schizonts and lastly, differentiates into merozoites again. The time it takes to complete a full blood life cycle, namely from merozoite to merozoite again, differs between the *Plasmodium* species.

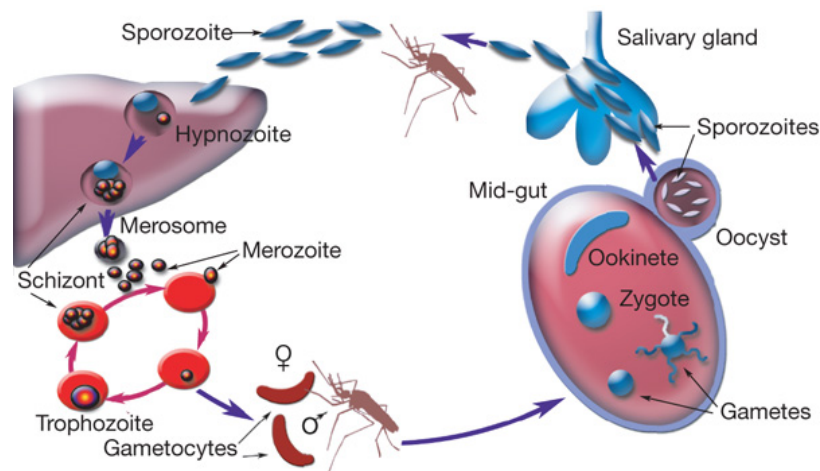


Figure 1.1: The diagram represents the conserved life cycle of *Plasmodium* taken from Winzeler (2008). The full description of the life cycle is discussed in the text.

The protozoans responsible for world wide human malaria include *Plasmodium falciparum*, *Plasmodium vivax*, *Plasmodium ovale* and *Plasmodium malariae*. *P. falciparum* is responsible for 80% of malarial cases and responsible for 90% of malarial

related deaths, but recently, another human malaria has been discovered, *Plasmodium knowlesi*, with a life cycle closer to *P. berghei*, a murine malaria, than *P. falciparum* (Manguin *et al.*, 2010). The other murine malaria parasites include *P. chabaudi*, *P. vinckei* and *P. yoelii*, but *P. berghei* has been used as a popular model organism due to the ease of genetic engineering (Craig *et al.*, 2012).

Great improvements have been made in the field of antimalarial drug development in recent years: Fortuitous discoveries of drugs in the past has been replaced with side chain alterations to increase effectiveness or circumvent resistance. The increased need for novel drugs led to the development of improved drug design using side-effect similarity (Campillos *et al.*, 2008). The nature of organisms to inexorably gain resistance to our novel drugs resulted in the exploration of soft drug design. The aim of this approach was to develop safer drugs by considering the effects of the metabolism when creating metabolites that inactivate enzymes to elicit a therapeutic response (review by Bodor and Buchwald (2000)). Discoveries in the field of integrated metabolic modelling and analysis opened up new possibilities to find weaknesses in organisms. By performing metabolic control analysis (MCA), an enzyme that dominates the flux could be identified and exploited (Snoep *et al.*, 2015). The combined work of Gerald Penkler, Francois du Toit and Francois Brand from the Molecular and Systems Biology lab at the University of Stellenbosch created a combined working model for the metabolism of *P. falciparum* and the human RBC, that lead to the successful identification of a potential drug target, namely the parasitic hexose transporter (Snoep *et al.*, 2015).

The goal of this thesis was to test the feasibility of creating a whole body model capable of describing the progression of the malarial infection and it's effect on the body's physiological state on a metabolic and biochemical level. The feasibility of the model will be measured by the ability of the model to predict the intercellular concentrations of the metabolites and the flux of the glycolytic pathway. For this research project, rats were infected with *P. berghei* to test the feasibility of creating a model that could potentially describe the metabolic changes resulting from the infection. A basic model had to be constructed, but to do so the following objectives had to be completed:

1. Infect Wistar Rats with *P. berghei*, ANKA strain, and obtain blood glucose and lactate data for the progression of the malarial infection whilst measuring the ability of the rat to maintain homeostasis of the blood glucose and lactate after incurring small perturbations
2. Isolate the parasites from the RBCs and subsequently lyse the cells to free the enzymes.
3. Measure the kinetic parameters of the intercellular enzymes of the *P. berghei* parasite
4. Use the kinetic parameters of the different enzymes to produce a working model of the glycolytic pathway

The outcomes of the objectives will be discussed in the three research chapters. Each chapter will contain introduction, methods and materials and results and

discussions sections for the respective experiment and outcome. Chapter 2, entitled "Rat blood analysis", will discuss the infection of the rats, the obtaining of the blood glucose and lactate, the pulse experiments, the measuring of the blood glucose and lactate, parasitemia and haematocrit measurements and the results obtained from the measurements. In chapter 3, "Enzymes kinetics", the method of extracting the enzymes as well as performing the enzyme kinetic studies will be discussed. The introduction and methods and materials for chapter 3 include detailed information on enzyme isolation, the enzymes in question and enzyme characterization. Results of the enzyme characterization is discussed at the end of chapter 3. Metabolic model construction is covered in chapter 4, named "Model creation". The methods for the model creation is discussed along with the equations used for the glycolytic model. Finally, the thesis concludes with a discussion chapter, chapter 5, which will discuss the feasibility of the model and the possibility of creating a full body model and the requirements thereof.

Chapter 2

Rat blood analysis

2.1 Introduction

In this study, we attempt to assess whether creating a whole body model is feasible. The feasibility would depend on our ability to measure different blood parameters our ability to fit rate equations to the kinetic data sets to adequately describe the perturbations the malarial infections would make to the normal blood values of a rat. Should such a study prove possible, a model could be created and adjusted for human anatomy to be used as a drug target identification or a diagnostic tool.

Ultimately, the goal of the rat studies was to create a whole body model that is capable of mathematically predicting the change in blood glucose and lactate levels based on kinetic values of the rats' blood glucose and lactate homeostatic potential and the malarial parasites' use of nutrients in the blood. Such a model could be used to determine the extent of infection. Combining a detailed kinetic model of the metabolisms of the malarial parasite and red blood cell could potentially lead to the uncovering of a weakness in the malarial parasite. To identify a weakness, metabolic control analysis needs to be performed to identify the enzymes with the dominant control over the system's flux whilst being sufficiently different from the RBCs homologues enzyme. Figure 2.1 displays a simplified diagram that describes the changes in blood glucose and lactate as a result of the rat's and the malarial parasite's metabolisms. Equation 2.1 and 2.2 forms the foundation for the simplified model adapted from Sorensen (1985) with λ being the body's ability to produce, p, or consume, c, glucose or lactate and ϵ the malarial parasite's ability to consume glucose and produce lactate.

$$dglu = \lambda_{glu-p} - \lambda_{glu-c} - \epsilon_c \quad (2.1)$$

$$dlac = \lambda_{lac-p} - \lambda_{lac-c} + \epsilon_p \quad (2.2)$$

The above equations could be dissected further to include the parameters that change the production and consumption rates of both the malaria parasite's and body's metabolisms. The resting glucose consumption of a body is influenced by the insulin-blood glucose ratio, whilst the body's resting production of glucose is dependent on the insulin concentration and the basal glucose production rates (Parker

et al., 1999). Both the glucose production and glucose consumption rates are influenced by the haematocrit with lower haemoglobin concentrations increasing the glucose turnover rate (Henderson *et al.*, 1986). Resting lactate production and consumption rates depend on the body's basal rates as well as the oxygen concentration in the blood. Malarial consumption of glucose and production of lactate would predominantly depend on the parasitemia (parasites per RBC in the blood), glucose concentration in the blood and oxygen concentration in the blood (Bowman *et al.*, 1960). For simplification of this study, it is assumed that the malaria parasites only utilizes anaerobic glycolysis and would produce 2 units of lactate per unit of glucose consumed.

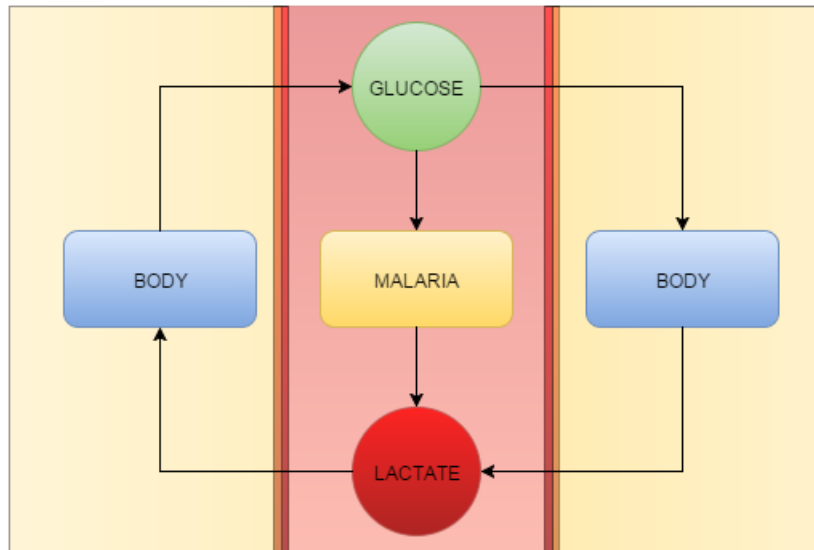


Figure 2.1: Simplified schematic of influences of blood glucose and lactate. The schema portrays a simplified view of the metabolism of the body that removes lactate or glucose from the blood and converts it to glucose and lactate respectively. The malaria parasite utilizes glucose as a carbon fuel source and converts the sugar to lactate in the blood.

The first set of experiments was to test the feasibility of measuring changes in the blood, which include the parasitemia, the haematocrit (amount of RBCs per unit volume of whole blood (unaltered blood)), blood glucose and blood lactate concentrations. During the course of the infection, parasitemia would be expected to increase exponentially as one parasite could release multiple merozoites to reinfect more RBCs and continue the asexual cycle of malaria. The exponential growth, as with all parasitic organisms, would be dependent on the abundance of nutrients, the growth conditions, the influence of the host's immune system and the availability of cells to infect. Since *P. berghei* infects and ruptures murine RBCs, one would expect to see an increase in the amount of parasites in the blood, but a decrease in the amount of RBCs. Because of the rupturing of the RBCs, the haematocrit should decrease proportionately to the increase of the parasitemia if no other RBCs are created. The rate of increase of parasitemia per day could therefore be calculated if the rate of haematocrit decay is known. The proportionality of parasitemia and

haematocrit was tested in this study to see if it is feasible to create a model that could describe the growth of the parasite along with the decay of the RBCs.

Malaria, being a voracious consumer of glucose to produce lactate, is known for causing lactic acidosis (acidifying of the blood by introduction of excessive amounts of lactate into the blood) (Holloway *et al.*, 1995). The increase in blood lactate and decrease in blood glucose could indicate the extent of the malarial infection (parasitemia)(Holloway *et al.*, 1991). The relationship of blood glucose and blood lactate was then tested in this thesis to assess if creating a mathematical model could describe the changes in the blood concentrations and the parasitemia.

Changes in blood glucose and lactate is not only dependent on the parasitemia, but also the body's ability to maintain homeostasis. Homeostasis is regulated by a complex network of organs and hormones and could prove too complex to describe mathematically, but for this study, we set out to assess the feasibility of measuring the homeostatic potential of the rat's metabolism by perturbing the blood glucose and lactate concentrations and measuring the time it took for the metabolism of the rat to return the blood concentrations to normal. The extent of the infection could influence the rat's homeostatic potential, from the acidifying of the organs and increased glucose turnover rate from the increase in parasites, which could be modelled mathematically (Haque *et al.*, 2011). The model would then be capable of predicting the changes in blood glucose and lactate as a function of the parasitemia.

The aim of this chapter was to investigate the feasibility of the above mentioned potential relationships. To test this, we looked at the possibility of measuring the parasitemia and haematocrit. The relationship between the two variables was then scrutinized. Blood glucose and lactate determination was then investigated and the correlation between the concentrations and the parasitemia analysed. Should all the experiments conclude that the relationships could be described mathematically, the creation of a mathematical model would be deemed plausible and the feasibility of the study warrants further investigation.

2.2 Methods and Materials

2.2.1 Materials

For increased accuracy and consistency, all the chemicals used in the experiments were purchased from Sigma-Aldrich unless otherwise stated in text. ANKA strain malaria was obtained from Grootte Schuur hospital in Cape Town and the rats were obtained from Stellenbosch university, Tygerberg campus.

2.2.2 Ethical Clearance

Ethical clearance to perform the study on rats was obtained on the 24th of August 2013, along with Biohazard clearance, from the faculty of health sciences animal research ethics committee, University of Cape Town (Application 014/006).

2.2.3 Innoculation and acquisition of the rats

A summary of the experimental design is displayed in figure 2.2. Albino Wistar rats, aged 5-6 weeks, with a mean body mass of ± 200 g were purchased from Tygerberg Hospital in Bellville, South Africa. Older rats seem to not be afflicted by malarial infection after inoculation. The rats were given 3 days to acclimatize to the new environment. On the last day of acclimatization, blood was drawn from the rats' tails to measure the basal blood glucose and lactate concentrations as well as the haematocrit. 15 rats were inoculated with 1×10^6 *P. berghei*, ANKA strain, into the penile vein, slightly less than the amount found to cause 100% mortality (Pedroni *et al.*, 2006). The inoculate was drawn from 2 donor rats that were infected prior to the start of the experiment.

2.2.4 Daily blood sampling

During the course of the experiment (day 2 till day 12), blood was drawn from the rats daily. A small tube was used to trap the rats to simplify drawing ± 200 μ l of whole blood from the tail of the rats using a 21 gauge needle. Whilst the wound still bled, blood from the needle wound was applied to a clean microscope plate for parasitemia measurements. 20 μ l of the drawn whole blood was aliquoted into a separate tube along with 5 μ l anticoagulant, CPDA fluid (Appendix A), for haematocrit measurements. The remaining blood was then centrifuged using a desktop centrifuge (Prism Mini centrifuge, $2000 \times g$) for 1 minute and two sets of 50 μ l plasma supernatant were removed and placed in different tubes for separate lactate en glucose concentration determinations. All the rats were euthanised 12 days post inoculation to minimize animal suffering.

2.2.5 Determining parasitemia with microscopy

During the daily blood collection, a drop of blood from the syringe of each infected rat was placed on a microscope slide and smeared. After the blood smear was completely dry, the blood was fixed by inundating the slide with methanol for 30 seconds. The methanol covering the slide was then washed away with water and

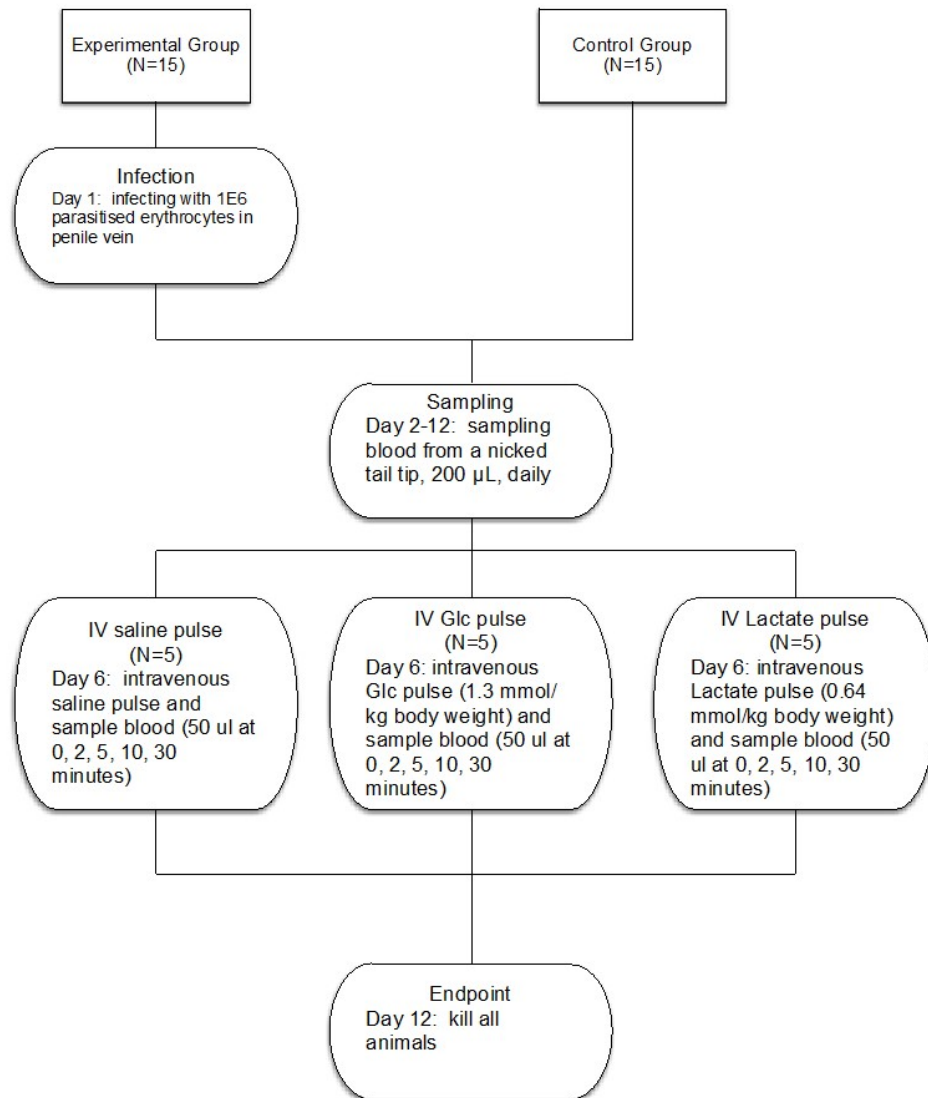


Figure 2.2: Experimental design for the *in vivo* rat study. The figure graphically describes the course of the experiments done on the rats. The total duration of the experiment was 12 days, starting with 30 uninfected rats of which 15 were inoculated with *P. berghei* and 15 kept as a control group. The different elements of the flow chart describe the events of the different days.

dried. Diluted (1:9 in PBS) Giemsa's stain solution (Merck (Pty) Ltd, Germany) was used to cover the fixed smear for approximately 10 minutes. The Giemsa's stain was washed off with water and completely dried before viewing the slide under a microscope. Three different photos were taken of each slide for counting. Percentage parasitemia was calculated by counting the total number of RBCs in the photos, counting the total number of parasites, including multiple parasites per RBC, and dividing the amount of parasites with the total number of RBCs.

2.2.6 Determining haematocrit with microscopy

The 25 μl samples of each rat drawn daily, consisting of 20 μl whole blood and 5 μl CPDA fluid, was diluted (1:1). From the dilute, $\pm 10 \mu\text{l}$ is injected into a Marienfeld improved Neubauer counting chamber and placed under a microscope for counting. Total intact RBCs from 5 inner haemocytometer counting chambers was counted. The average from the 5 counts was then used as the haematocrit of the rat on that day post inoculation.

2.2.7 Blood glucose concentration determination

Daily blood glucose concentration of each rat was determined enzymatically using a BioTek Powerwave 340 spectrophotometer. A glucose determination cocktail was created for the measurements, which contained 2.5 mg/ml adenosine triphosphate (ATP), 0.5 mg/ml nicotinamide adenine dinucleotide phosphate (NADP^+) and 10 $\mu\text{l}/\text{ml}$ HK/G6PDH (hexokinase/glucose-6-phosphate dehydrogenase mixture), linking enzyme, in glucose-lactate determination buffer (GLDB, Appendix A). In a well of the microplate, greiner 96-well plate, 5 μl of 1:1 diluted sample or glucose standard (0 - 10 mM used as a internal standard) was added with 95 μl of glucose determination cocktail and the absorbance measured at 340 nm with the spectrophotometer after a 15 minute incubation at room temperature. All samples were measured in triplicate.

2.2.8 Blood lactate concentration determination

Blood lactate concentrations from each infected and uninfected rat was determined enzymatically using a BioTek Powerwave 340 spectrophotometer. A lactate determination cocktail was created for the measurement, which contained 40 $\mu\text{l}/\text{ml}$ Hydrazine, 4 mM NAD^+ and 2 $\mu\text{l}/\text{ml}$ lactate dehydrogenase (LDH), as linking enzyme, in GLDB (Appendix A). In a 96 well Greiner plate, 5 μl of sample or lactate standard (0 - 20 mM) was added with 95 μl of the lactate determination cocktail. The plate was incubated for 90 minutes at room temperature and kept away from light contact before placing it in the spectrophotometer to measure the absorbance at 340 nm. All samples were measured in triplicate.

2.2.9 Pulse experiments

On day six post inoculation, the pulse experiments were performed. Of the 15 rats, 3 groups of 5 rats each were used from both the infected and uninfected rats for the pulse experiments. The 3 groups were injected with either saline solution, 1.3 mmol/kg body weight glucose or 0.64 mmol/kg body weight lactate. To increase the accuracy of the experiments and to minimize suffering of the animals, the animals were anaesthetized with 4% isoflurane during the experiment. Blood sampling (50 μl per sampling) was drawn before the injection, 2, 5, 10 and 30 minutes after the injection. The whole blood sample was then centrifuged using a desktop centrifuge (Prism Mini centrifuge, 2000 \times g) for one minute. A 20 μl supernatant was then removed and aliquoted into two tubes; 10 μl per aliquot for glucose and lactate determination as outlined above. Deviating from the standard blood glucose

and lactate determinations described in this section, the samples were measured in duplicate.

2.2.10 Computational analysis and statistics

The enzymatic and microscopical data obtained were interpreted using GraphPad Prism version 5.0 and the statistical analysis performed with the same program. The graphs were produced with Wolfram Mathematica version 10.0.

2.3 Results and Discussion

2.3.1 Parasitemia

The first set of experiments was conducted to assess if measuring the parasitemia is possible and if an equation could be fitted to the rate of increase in parasitemia over the course of the infection. Considering a full blood cycle of a RBC infected with a single merozoite could release between eight and sixteen merozoites, exponential growth is expected to be observed during the course of the infection (Killick-Kendrick, 1974). An example of the photos taken from the slides as well as the progression of the malarial infection is given in figure 2.4. Figure 2.3 A shows the results from the average parasitemia measurements as a function of time in days and an exponential curve can be observed. Using the log of the average parasitemia, Figure 2.3 B, as a function of time (day) a linear correlation ($p < 0.0001$) is observed. From the logarithmic linear growth curve, a doubling time of 1.98 days is calculated, but true growth modelling is too complex for this thesis, as the growth is dependent on numerous factors (discussed later in this thesis). The elements that could be responsible for the lower than expected growth rate include a sub-optimal growth if a RBC is infected with multiple merozoites, selectivity for immature erythrocytes, immune system counteracting the growth, the creation of more erythrocytes and the time-dependent loss of invasive ability of the merozoites (McAlister (1977), Bannister *et al.* (1975)). The full set of parasitemia measurements for all the rats is displayed in figure B.1. The full data set shows that the rate of increase in parasitemia is variable between the rats and that an average of the parasitemia is a better measuring tool for model creation.

2.3.2 Haematocrit

The rupturing of the RBCs to release the merozoites during the asexual blood cycle could lead to a decrease in the total haematocrit of the rats. The haematocrit of the infected rats were measured to assess the feasibility of finding a correlation between the increase in parasitemia and haematocrit. Average haematocrit of all 15 infected rats is displayed on figure 2.5 with graph A depicting the average haematocrit as a function of time (days). A linear correlation ($p < 0.01$) exists between the decline of the haematocrit and course of the infection (line not shown). Figure 2.5 B shows the average haematocrit as a function of the log of the average parasitemia. Another linear correlation ($p < 0.01$) exists between the average haematocrit and the log of

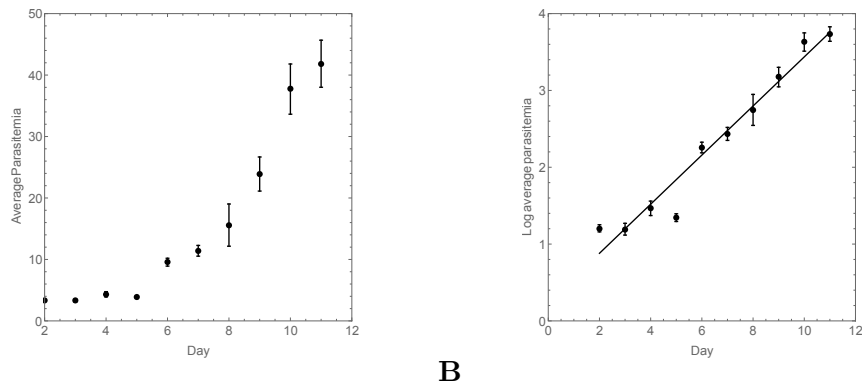


Figure 2.3: Results from the parasitemia measured represented as average parasitemia over the course of the infection. The two graphs represent the average parasitemia of the rats per day (A) and the log of the average parasitemia of the rats (B) per day post inoculation. The average parasitemia shows a clear exponential curve which is confirmed by fitting a straight line to the log of the average parasitemia ($p < 0.0001$). The full set of parasitemia values are given in figure B.1 for both the average parasitemia and the log of the average parasitemia.

the average parasitemia (line not shown). A true mathematical relationship between parasitemia and haematocrit is too complex to equate in this thesis, but a linear correlation for both graphs is statistically true. The change in haematocrit could be studied further by including the body's ability to create new RBCs and by separating the reticulocytes from the eurythrocytes to study the effect of the preference for immature RBCs and to create a model for the change in haematocrit during the course of an infection (Janse and Waters, 1995). A haematocrit minimum of $\pm 20\%$ was observed in 2.5. If the haematocrit decreased any further, it would result in the death of the rat. Measuring the haematocrit could therefore serve as a viable diagnostic tool to measure the extent of the malarial infection and could lead to a method to prioritise the healthcare of critically ill malaria patients if a mathematical relationship exists between haematocrit and other blood parameters (parasitemia, blood pH, blood glucose concentration ect.). The full set of haematocrit measurements for all the rats is displayed in figure B.2 in appendix B. The full data set does not provide any further insight into rate at which the haematocrit decreases during malarial infections.

2.3.3 Blood glucose and lactate

A validated and working full body model would be able to predict the changes of blood glucose and lactate during the course of the infection. Since *P. falciparum* consumes glucose at a rate of between 50 and 100 times that of uninfected human RBC, it could be assumed that *P. berghei* will follow a same trend (Roth Jr, 1989). We set out to assess if measuring the blood glucose and lactate concentrations is possible and to find a link between the concentrations and parasitemia. High parasitemia would be expected to lead to a lower blood glucose concentration and an increased blood lactate concentration as the 60 to 70% of glucose is converted to lac-

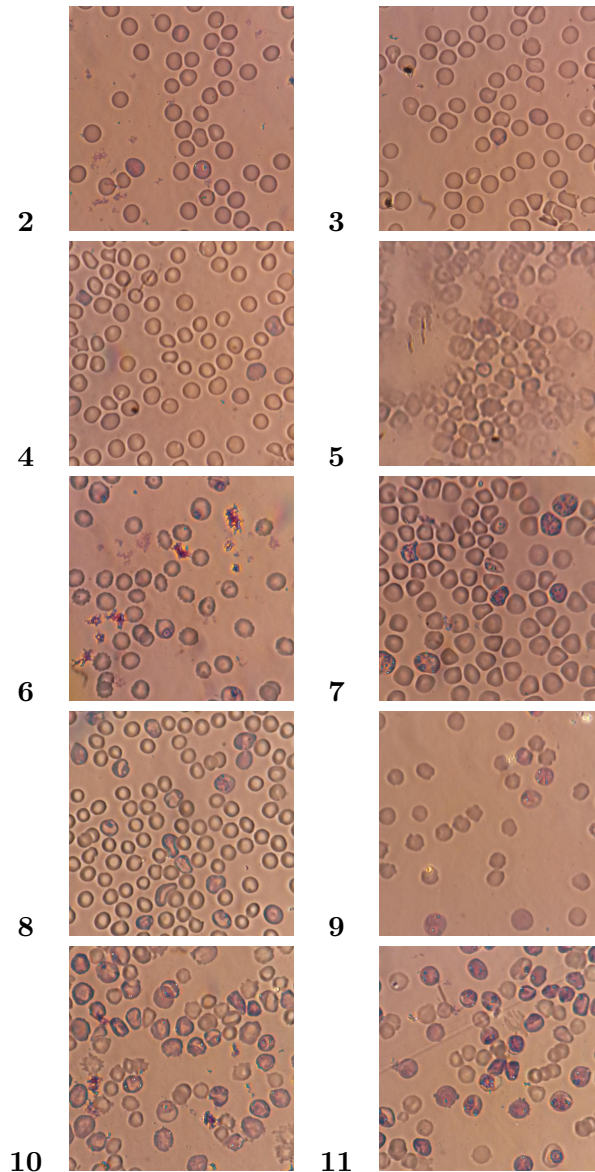


Figure 2.4: Blood slides of a rat over the course of the infection. An example of the blood slides taken each day, represented by the numbers next to the pictures, is displayed in this figure. Counting the parasites, coloured blue by Giemsa's stain, in the RBCs and dividing by the total amount of RBCs in the slide gives an approximate parasitemia for the rat.

tate and transported out as lactate (Jensen *et al.*, 1983). A study done by Holloway *et al.* (1995) shows that a rat's body is able to maintain nominal homeostasis for lower concentrations of parasitemia, but after a certain threshold ($\pm 20\%$), the blood glucose concentration decreases to a minimum of $\pm 2\text{mM}$ and blood lactate increases to $\pm 12\text{mM}$. Results from this project show a similar trend to that of the study with regards to the decrease of blood glucose and blood lactate, displayed in figure 2.6, but several differences are evident from the data obtained. Plotting the blood lactate concentration as a function of the log of the parasitemia, Figure 2.6 A, does not convey a clear correlation between the concentration of the blood lactate and

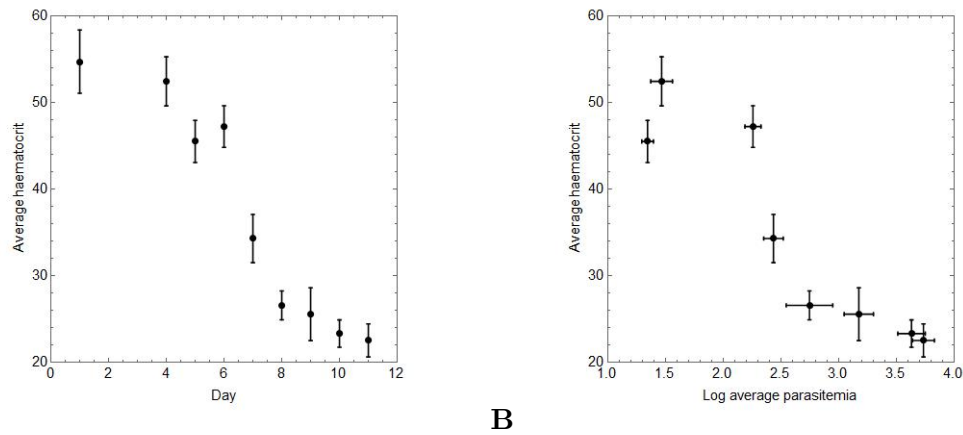


Figure 2.5: Results from the haematocrit measurements represented as average haematocrit over the course of the infection. The average haematocrit over the course of the infection is displayed as a function of days post inoculation (A) and log of the average parasitemia (B). As expected, the haematocrit decreased over the course of the infection, reaching a minimum of $\pm 20\%$ haematocrit. Lowering the haematocrit any further, would result in the death of the rat. A full set of haematocrit measurements for each rat represented as both a function of time and parasitemia is displayed in figure B.2.

the extent of the infection. When blood lactate is plotted against the parasitemia interval (intervals of 10%), Figure 2.6 C, the influence of parasitemia becomes more visible with low blood lactate concentration at low of parasitemia (20% to 30%) and great increases in blood lactate concentration above 60% parasitemia. The reason for the initial decrease in blood lactate could be a result of the adaptation of the rat's body's metabolism to prioritize lactate consumption as there is a constant influx of lactate from the parasites. The decrease in blood glucose concentration, Figure 2.6 B, shows a linear correlation ($P < 0.0001$ significantly non-zero slope) when plotted against the log of the parasitemia. Figure 2.6 D does not show a clear correlation between the interval of parasitemia (intervals of 10%) and the blood glucose concentration, but it should still be noted that higher concentrations of parasitemia of greater than 40% has a lower blood glucose than the blood glucose concentration of uninfected rats. A possible reason for the large variation in concentrations could be due to the panicked state in which the animals presented themselves whilst the blood was drawn. Future studies may necessitate anaesthesia for all the interactions with the rats to increase accuracy of the experiments. Another valuable tool to be used for the change in blood glucose and lactate levels could include the measuring of the blood pH as the amount of lactate in the blood correlates to the acidifying of the blood, since it has been reported that blood pH go down to as low as 6.98 from 7.23 in mice with 86% parasitemia (Kruckeberg *et al.*, 1981).

2.3.4 Pulse Results

Construction of a whole body model requires knowledge of the homeostatic potential of rats body. The aim of this experiment therefore to assess the feasibility of

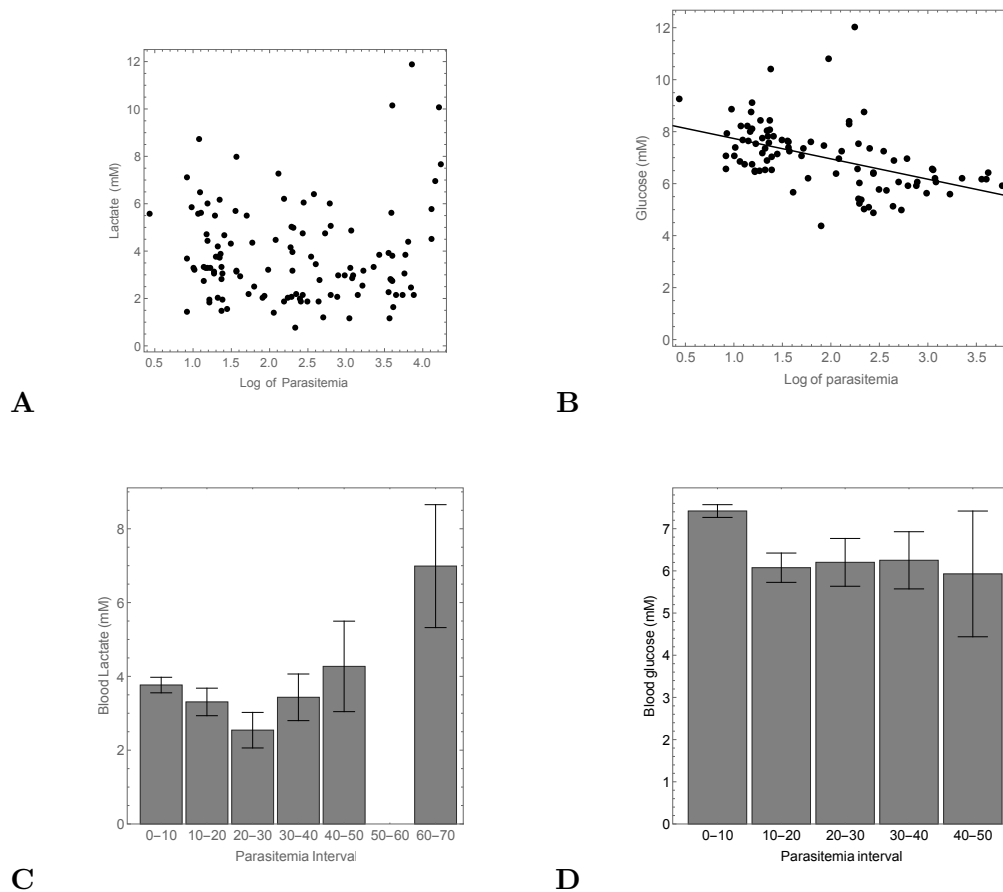


Figure 2.6: Blood glucose and lactate concentrations over the course of the infection displayed as a function of parasitemia and parasitemia interval (% parasitemia). The blood lactate (A) and glucose (B) concentration (mM) for the infected rats is shown as a function of the log of the different parasitemia's for the rats. The lactate concentration does not show a clear correlation to the log of the average parasitemia, while the blood glucose shows a linear correlation ($p < 0.01$) to the log of parasitemia. The glucose concentration for the different parasitemia intervals (D) does not show a clear correlation, but the lactate concentration (C) for the different intervals shows an increase with high parasitemia intervals. Data could not be obtained for the blood lactate concentration between the interval 50 to 60% parasitemia. The full data sets for each rat is shown as a function of parasitemia (figure B.3) and day post inoculation (figure B.4) in Appendix B.

measuring the homeostatic potential by perturbing the blood glucose and lactate levels by performing pulse experiments. The glucose pulse experiments for both the infected and the uninfected rats (figure 2.7 A and B respectively) displayed a classic one phase decay curve over a period of time, returning to nominal blood glucose concentrations after ± 30 minutes ($P < 0.01$ for the uninfected rat glucose pulse) similar to the results of Tsutsu *et al.* (1989). Both the lactate and glucose pulse experiments did not yield any definitive influence by the infection, as no significant differences can be observed between the infected and uninfected rat glucose pulse

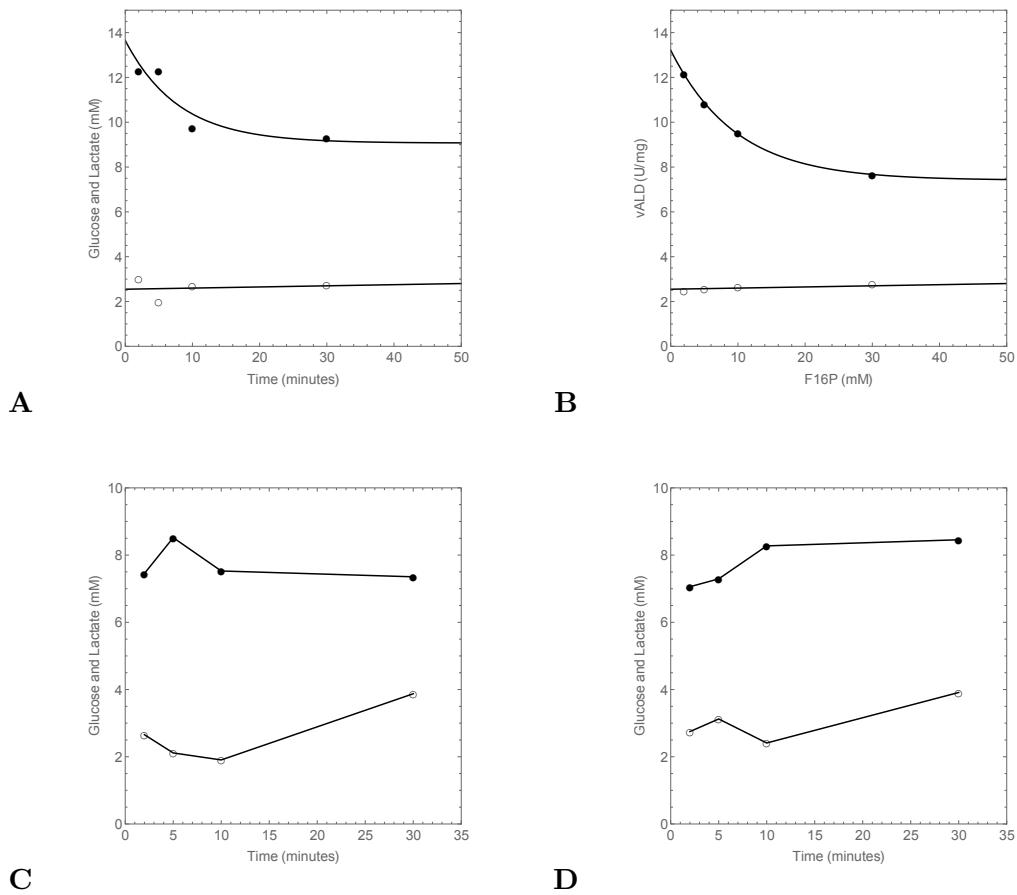


Figure 2.7: Blood glucose and lactate concentration from the pulse experiments for the infected and uninfected rats. The data from the glucose pulse experiments for both the infected (A) and uninfected (B) rats is shown as a function of time (minutes). Closed circles represent the blood glucose concentrations and open circles the blood lactate concentrations. A one phase decay is fitted to both graphs for the glucose concentration and a straight line is fitted to the lactate concentration. The data from the lactate pulse experiments for both the infected (C) and uninfected (D) rats is shown as a function of time (minutes). No discernible correlation could be seen from the lactate pulse experiments.

experiments. The lack of correlation could be due to the low parasitemia (average of 9.55% parasitemia) during the pulse experiments. Using a higher parasitemia, larger variation in the parasitemia or a range of glucose concentrations could lead to a better understanding of the homeostatic potential of the rat's metabolism. During the glucose pulse experiment, the blood lactate concentration did not seem to change significantly which could be due to the parasitemia not being adequate to convert significant amounts of glucose to lactate. No conclusions can be drawn from both the infected or uninfected lactate pulse experiments displayed in figure 2.7 C and D respectively. Blood glucose concentrations remained largely unchanged during the experiments, whilst lactate seems to increase during the course of the lactate pulse. The reason for the increase in blood lactate concentration could be

due to overcompensation of lactate removal, but the true reason is not known. One conclusion that can be drawn for both the glucose and lactate pulse experiments is the need for repeats of these experiments with higher parasitemia, ideally $\pm 50\%$, to reach more definitive results. Since this study is on the feasibility of creating a whole body rat model, the glucose pulse experiment was successfully performed, suggesting that such a pulse experiment is possible and could provide researchers with valuable information on the homeostatic capabilities of the rats.

2.3.5 Summary

The measuring of parasitemia, haematocrit and blood glucose and lactate was successfully. Furthermore, a relationship between the different parameters was identified in this chapter, providing evidence that the construction of a whole body model is feasible. Since we could determine exponential decay back to starting blood glucose concentrations, the glucose pulse experiments proved successful. Interestingly, there was no increase in the blood lactate concentrations after the glucose pulse and the glucose consumption in infected and non-infected rats were very similar. The lactate pulse was not so successful, since no increase in lactate was observed immediately after the pulse. This could be due to having used too small a concentration of lactate, or due to a very rapid lactate consumption rate. Strategies to improve on the pulse experiment includes performing the experiment with a range of pulse concentrations and performing the pulses at a larger parasitemia. Since the blood analysis proved feasible, the possibility of constructing a metabolic model was investigated for a complete whole body model in chapters 3 and 4.

Chapter 3

Enzymes kinetics

3.1 Introduction

A model that is only capable of describing the physiological response to an increase in parasitemia lacks the depth needed to describe the influences of the metabolism of the malarial parasite and the enzymes making up the different metabolic pathways. Metabolic models have been constructed for different organisms, including *S. cerevisiae* and *P. falciparum* (Teusink *et al.* (2000), Snoep *et al.* (2015)). The constructed models were not only capable of predicting the flux and steady state metabolite concentrations, but were also capable of describing the effect inhibiting one enzyme would have on the system as a whole, serving as a viable tool for drug target identification. To create a model, the mechanism (kinetic parameters) of each enzyme needs to be quantified in terms of the velocity with which each enzyme could catalyse reactions in the system. Once the kinetic parameters are quantified, the different enzymes could be combined to create a model.

Research done on *Plasmodium spp.* showed that, although many of the biosynthesis pathways are omitted in the parasites, the core conserved metabolic pathways remain, including glycolysis, the pentose phosphate pathway, lipid biosynthesis and parts of the tricarboxylic acid cycle (TCA) (reviewed by Olszewski and Llinás (2011)). The majority of the auxiliary metabolic pathways, excluding glycolysis, are found to form part of biosynthesis and not catabolism. The apparent inability of the auxiliary pathway to perform catabolism could be due to the over abundance of resources, both from the blood serum, glucose, and the breakdown of haemoglobin from the RBCs to produce amino acids.

Since between 60 and 70% of glucose is converted to lactate, the remaining glucose is presumed to flow into the pentose phosphate pathway (PPP) (Jensen *et al.*, 1983). Atamna *et al.* (1994) found that infected RBCs have PPP activity 78 times greater than that of the uninfected RBCs and the parasite has a PPP activity 24-fold greater than that of the RBC, which serves as affirming evidence that the PPP is essential for the survival and growth of the parasite. Two major reasons for the use of the PPP is the production of NADPH via the oxidative branch, used to combat oxidative stress, and the creation of ribulose-5-phosphate for use in the purine metabolism to synthesise nucleotides (Roth Jr *et al.*, 1986). Degradation of haemoglobin releases reactive oxygen species, including H_2O_2 and free haem, which

causes oxidative stress (Becker *et al.*, 2004). Reduced glutathione (GSH) is used to reduce the oxidative radicals which in turn creates oxidized glutathione disulphate (GSSG). GSH thus offers oxidative protection for both the RBC and the parasite. NADPH, produced from the PPP, is used as reducing agent to reduce GSSG and restore the GSH balance. The non-oxidative branches uses fructose-6-phosphate (F6P) and glyceraldehyde-3-phosphate (GAP) from glycolysis as the substrates to be converted to sedoheptulose-7-phosphate and erythrose-4-phosphate.

Although the malarial genome contains all the genes encoding for mitochondrial enzymes, the role of the enzymes aren't well understood (Fry and Beesley, 1991). The creation of acetyl-CoA, via purine salvage pathway mediated by the tricarboxylic acid (TCA) cycle used in lipid metabolism, appears to be the purpose of the expressed TCA enzymes in *Plasmodium* (reviewed by Van Dooren *et al.* (2006)). The asexual stage malarial parasite lacks the enzyme pyruvate dehydrogenase needed to convert pyruvate to acetyl-CoA to initiate the TCA cycle (Pei *et al.*, 2010). Oxaloacetate, an intermediary step for the interconversion between aspartate and malate, is formed via phosphoenol pyruvate (PEP) carboxylase and could influence the total amount of lactate produced by siphoning PEP away as part of a carbon fixation pathway (McDaniel and Siu, 1972). For the purpose of this study, the TCA cycle and PEP decarboxylase were assumed to not influence the use of glucose or production of lactate.

Investigating the feasibility of measuring the velocity and calculating the kinetic parameters of the glycolytic enzymes was the focus of this chapter. The aim was to characterize all 11 enzymes in the glycolytic pathway of *P. berghei*. Substantial proof for the feasibility of creating a model will exist if the characterization of the enzymes are possible.

3.1.1 Kinetic parameter quantification

A simplified schema of the glycolytic pathway is presented in figure 3.1. Glucose is converted to lactate by 11 enzymatic steps. *Plasmodium spp.* lacks the enzymes necessary to undergo gluconeogenesis, except for phosphoenolpyruvate carboxylase, which is thought to be used for carbon fixation (Hayward, 2000). The analysis of the enzymes involved measuring the different specific activities (maximal velocity of the reaction normalised to protein concentration) for different substrate, product and inhibitory concentrations. Michealis-Menten equations are needed to describe the change in specific activity of the enzymes (Atkins and Nimmo, 1975).



The simplified reaction (eq. 3.1) illustrates a simple reaction where a substrate, S, that is converted to metabolite, X, and then converted to product, P. The conversions are done in two steps, named v_1 and v_2 , which can be adapted to equate the rate at which X is produced or consumed. The rate of the irreversible first reaction, v_1 , could be quantified with a standard irreversible Michaelis-Menten equation (eq. 3.2) (Goudar *et al.*, 1999). A reversible reaction, eg. v_2 , requires the incorporation of both the forward, V_f , and reverse, V_r , maximal velocities into the standard uni-uni

Michaelis-Menten reaction (eq. 3.3). The reactions could be expanded to include substrate, product and allosteric inhibition.

$$v_1 = \frac{V_{max} \cdot [s]}{K_s + [s]} \quad (3.2)$$

$$v_2 = \frac{V_f \frac{[x]}{K_x} - V_r \frac{[p]}{K_p}}{1 + \frac{[x]}{K_x} + \frac{[p]}{K_p}} \quad (3.3)$$

Without purifying the different glycolytic enzymes, some of the enzymes could not be measured in either the forward or reverse direction. The limitation of maximal rate measurements was circumvented by using the Haldane relation (eq. 3.4) (Mellors, 1976). For a reaction to reach equilibrium, the forward and reverse reaction must be equal and, if the K_{eq} is known, the maximal velocity of the missing parameter could be substituted using the Haldane relation. All the enzymes were characterised in enzyme assay buffer (EAB, Appendix A) at a pH of 7.17 that resembles intracellular conditions. EAB does not necessarily allow for maximal activity of the enzyme, rather, a physiological activity.

$$\frac{[p]_{eq}}{[x]_{eq}} = K_{eq} = \frac{V_f K_p}{V_r K_x} \quad (3.4)$$

3.1.2 Glycolytic enzymes

3.1.2.1 Hexokinase

Hexokinase (HK, EC 2.7.1.1) catalyses the important first step in glycolysis to start the catabolism of glucose. The enzyme, also called ATP:D-hexose 6-phosphotransferase, transfers a phosphate from ATP to glucose to create ADP and glucose-6-phosphate (G6P). The HK from *P. Berghei* catalyses the reaction 35 times faster than normal uninfected mouse erythrocytes (Kumar and Banyal, 1997). Like most of the *Plasmodium* glycolytic enzymes, HK is coded on one gene with no isoenzymes during the asexual phase, which could be the reason for the improved functionality of the parasitic enzyme compared to the mammalian orthologue (Olafsson *et al.*, 1992). Kumar and Banyal (1996) biochemically characterised the 47 kDa *P. berghei* enzyme in cell-extract and found that HK has a ATP K_m of 2mM and 0.431mM for glucose. Although *P. berghei* can only use glucose as a hexose substrate, Sherman (1979) found that some species of *Plasmodium* can use other hexose sugars, specifically mannose. The reaction is considered to be irreversible, although Wisner and Schweiger (1985) reported that glucose-6-phosphatase concentration increases with maturation of *P. vinckei* which could convert glucose-6-phosphate (G6P) back into glucose.

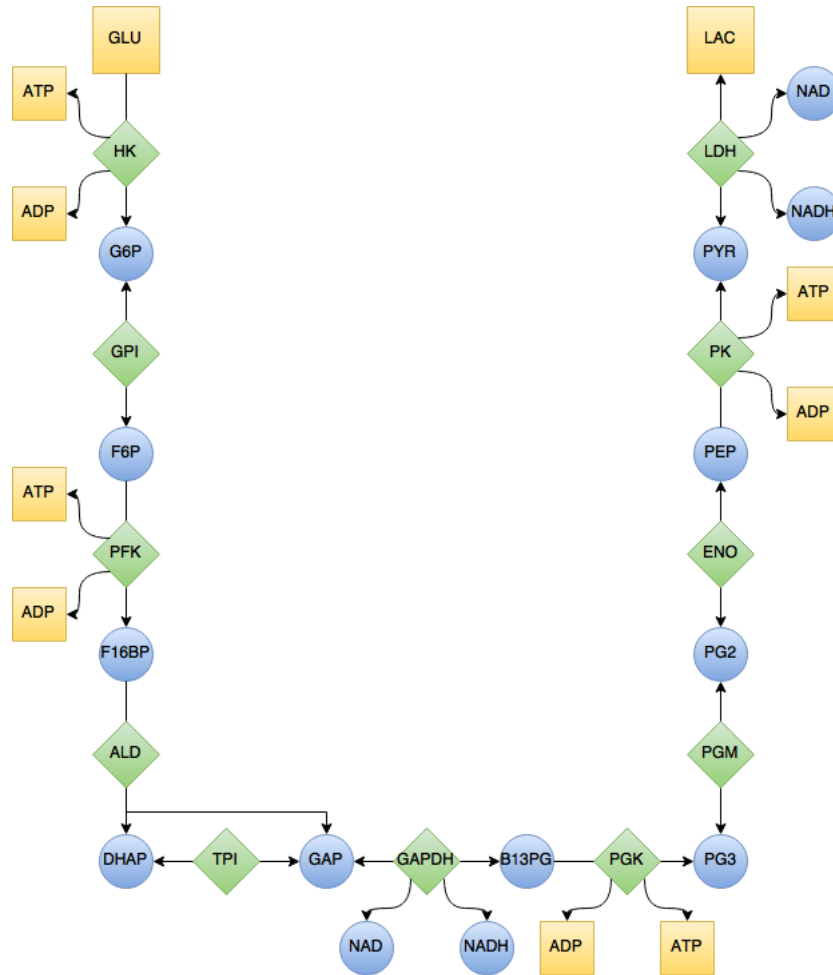


Figure 3.1: Simplified schema of glycolysis used to create the glycolytic model. The schema represents the classic view of glycolysis where glucose is converted to lactate by means of 11 enzymatic reactions. The shape of the different metabolites and enzymes represents the different roles in the model with the square representing a constrained metabolite, diamond an enzyme catalysed reaction and a circle represents a variable metabolite.

3.1.2.2 Glucosephosphate isomerase

Isomerization of G6P to fructose-6-phosphate (F6P) is catalysed by glucosephosphate isomerase (GPI, EC 5.3.1.9). Srivastava *et al.* (1992) purified the 66 kDa enzyme and found that *P. falciparum* has 3 or 4 isoenzymes which confers a 4 to 9 times greater GPI activity than uninfected RBCs. Inhibition of the enzyme has no effect on the host GPI, indicating that substantial differences exist between host and *Plasmodium* enzyme structure (Srivastava *et al.*, 1992).

3.1.2.3 Phosphofructokinase

The creation of fructose-1,6-bisphosphate (F16BP) and ADP from F6P and ATP is catalysed by phosphofructokinase (PFK), a key-regulatory enzyme in the glycolytic

pathway (Buckwitz *et al.*, 1990a). Extensive differences exist between the *Plasmodium* PFK and the erythrocytic native PFK. The different allosteric activation molecules is one of the major differences with erythrocytic PFK being activated by fructose-2,6-bisphosphate and AMP whilst *Plasmodium spp.* PFK is activated by PEP, F6P and Pi, while only being marginally activated by AMP (Jacobasch *et al.*, 1989). According to Buckwitz *et al.* (1990a), non-allosteric inhibition, as well as Mg-ATP binding site, competitive inhibition is observed with the addition of ADP; Furthermore, Buckwitz *et al.* (1988) observed increased inhibition of PFK by ATP with a decrease in pH. Buckwitz *et al.* (1990b) went further and described the effects of Mg-ATP, free ATP and Mg²⁺ on the activity of PFK and found that, whilst an increase in the substrate (Mg-ATP) does not inhibit the reaction, free ATP and Mg²⁺ inhibit the reaction allosterically. The size, structure and genetic code of the enzyme have yet to be elucidated.

3.1.2.4 Aldolase

The aldol-cleaving of F16BP to form dihydroxyacetone phosphate (DHAP) and glyceraldehyde-3-phosphate (GAP) is mediated by fructose-1,6-bisphosphate aldolase (ALD). Fructose-1-phosphate is cleaved by ALD as well but at a slower rate than F16BP. Two virtually identical ALD isoenzymes exist, ALD-1 and ALD-2, but ALD-1 (40.1 kDa) is expressed in sporozoite stage while ALD-2 (39.8 kDa) is expressed during the asexual blood cycle (Meier *et al.*, 1992). X-ray analysis of ALD crystal structure from *P. falciparum* revealed that ALD is a homotetrametric protein with a molecular weight of 160kDa (Kim *et al.*, 1998). Interestingly, the *Plasmodium* ALD enzyme differs extensively from the mammalian orthologue, complicating the classification of the enzyme into one of the three ALD classes (A, B and C).

3.1.2.5 Triosephosphate isomerase

The interconversion of DHAP and GAP, with enediol phosphate intermediate, is catalysed by triosephosphate isomerase (TPI). The 28 kDa enzyme of *P. falciparum* shows 42-45% homology to the eukaryotic isoenzymes, allowing for unique drug development (Younis *et al.*, 2014). Unlike the human TPI isomerase, the protein crystal structure reveals that the serine to phenolalanine mutation on residue 96 causes the enzyme to exist in two distinct conformations, namely open and closed catalytic loop, however, the influence the states have on the catalytic activity has not been elucidated (Parthasarathy *et al.*, 2002).

3.1.2.6 Glyceraldehyde 3-phosphate dehydrogenase

Glyceraldehyde-3-phosphate dehydrogenase (GAPDH, EC 1.2.1.12) catalyses the oxidation of GAP with NAD⁺ and inorganic phosphate to produce 1,3-bisphosphoglycerate (B13PG) and NADH. The 36.7 kDa of *P. falciparum* protein has been expressed in *Escherichia coli* and found to have 63.5% homology to the human erythrocytic counterpart (Srivastava *et al.*, 1992). The heteromeric protein consists of four identical polypeptide chains that, using sulphhydryl groups, catalyse the conversion with a hemithioacetal intermediate (Daubenberger *et al.*, 2000).

3.1.2.7 Phosphoglycerate kinase

The conversion of B13PG and ADP to 3-phosphoglycerate (3PG) and ATP is catalysed by 3-phosphoglycerate kinase (PGK, EC 2.7.2.3) with the help of Mg^{2+} and is the first reaction in the glycolytic pathway to produce ATP. Inhibition by anti-serum raised against the purified 45.5 kDa protein of *P. falciparum* does not influence the eurythrocytic counterpart, which is supported by the gene analysis that showed that only 60% similarity exists between the two enzymes (Grall *et al.*, 1992). Two isoenzymes exist for the 3PG in *P. falciparum*, but the asexual blood-stage parasite only produces a single 2.1 Kb mRNA transcript (Hicks *et al.*, 1991). The crystalline structure analysis and the biochemical characterization of the enzyme has been studied by Pal *et al.* (2004) and found that the enzyme is temperature sensitive and that suramin inhibits the working of the enzyme.

3.1.2.8 Phosphoglycerate mutase

Phosphoglycerate mutase (PGM, EC 5.4.2.1) catalyses the interconversion of 3PG to 2-phosphoglycerate (2PG). The crystal structure of one of the two putative isoenzymes of *P. falciparum* PGM was investigated by Hills *et al.* (2011), along with the biochemical characterization of the the isoenzyme. In the study it was found that PGM could dephosphorylate multiple metabolites, including F6P and F16BP, giving rise to the idea that PGM is a moonlighting enzyme with multiple functions (Gomez-Arreaza *et al.*, 2014).

3.1.2.9 Enolase

2PG to phosphoenol pyruvate (PEP) interconversion is catalysed by enolase (ENO, EC 4.2.1.11). As with PGM, ENO (51.4 kDa) is also known to be a moonlighting enzyme with non-glycolytic function (Pal-Bhowmick *et al.*, 2007b). The four isoforms of ENO, also 2-phospho-D-glycerate hydrolase, are thought to be due to the phosphorylating post transcriptional modification, which could give rise to the different functions of the enzyme. Pal-Bhowmick *et al.* (2004) biochemically characterised the homodimer of *P. yoelii* and found that Na^+ has an inhibitory effect, whilst K^+ and cofactor Mg^{2+} have an activation effect. A 68% identity and 78% homology exists between the *Plasmodium* and human orthologue ENO (Pal-Bhowmick *et al.*, 2007a).

3.1.2.10 Pyruvate kinase

The second ATP generating step in glycolysis is catalysed by the homotetramer, pyruvate kinase (PK). The 55.6 kDa enzyme converts ADP and PEP to ATP and pyruvate. Unlike most analogues of PK, the enzyme is not affected by F16BP or G6P, but inhibited by ATP and citrate. Chan and Sim (2004) overexpressed in *E. coli* and characterized PK and found that the affinity for ADP and PEP appears to be greater than that of the mammalian isoenzymes. Interestingly, a genetic PK deficiency confers resistance to malarial infection; The reason for the resistance is due to invasion defect of the erythrocytes and the preferential macrophage clearance (Ayi *et al.*, 2008).

3.1.2.11 Lactate Dehydrogenase

Lactate dehydrogenase (LDH, EC 1.1.1.27) catalyses the reduction of pyruvate and NADH to lactate and NAD⁺. A single 1.6 kB gene encodes for the 33 kDa enzyme that contains several distinct amino acid sequences to that of the eurythrocytic LDH. Bzik *et al.* (1993) expressed LDH in *Escherichia coli* and characterised the purified enzyme whilst (Vander Jagt *et al.*, 1981) performed partial purification and characterization from *P. falciparum* extract. LDH has been targeted as an inexpensive field diagnostic target by measuring the LDH activity in the presence of cofactor 3-acetyl puridine, a reaction that is very slow with RBC LDH but shows increase activity in parasite LDH (Makler and Hinrichs, 1993). Parasitemia calculation using 3-acetyl puridine and measuring LDH activity is comparable to using microscopy and 3H-hypoxanthine (Makler *et al.*, 1993)(Chulay *et al.*, 1983).

3.2 Methods and Materials

3.2.1 Materials

For increased accuracy and consistency, all the substrates, metabolites and enzymes used in the experiments were purchased from Sigma-Aldrich unless otherwise stated in text. The buffers used throughout this study, specifically the enzyme assay buffer (EAB), are described in Appendix A. The creators of the equipment used in this study is given in text.

3.2.2 Isolation of intact Parasites

The rats are euthanized followed by blood collection after reaching 12 days of infection or reaching critically low health. Critically low health criteria included paralysis, a comatose state, weight loss exceeding 15% of total starting weight, seizures, severe weakness, difficulty breathing and ataxia. Comas and paralysis are clear indicators of cerebral malaria, which is uncommon in Wistar rats, but not improbable (Kamiyama *et al.*, 1987). None of the rats used in this study suffered from cerebral malaria. Maximal sterile blood collection was made possible by using a method similar to cardiac puncture. The rats are anaesthetised with either 4% isoflurane and kept anaesthetized with 1.5% isoflurane or 100 mg/kg ketamine-xylazine. Ketamine-xylazine sedation proved difficult as the xylazine slows the heart rhythm and resulted in premature cardiac arrest (Hsu *et al.*, 1985). Blood sample collection was done through a method similar to cardiac puncture, but the blood was drawn from the caudal vena cava (Parasuraman *et al.*, 2010). Immediately after the blood collection, the collected blood is injected into a sterile tube with CPDA fluid (1 part CPDA to 7 parts whole blood) to stop the blood from coagulating. The collected blood could be used for either isolation of intact parasites or culturing in culture flasks.

Various *Plasmodium spp.* trophozoite isolation methods exist, including filter agglutination and lysis, glycerol-enhanced osmotic shock, saponin treatment and RBC-antibody lysis (Wongsrichanalai *et al.*, 2002). The saponin isolation method used for isolating the intact parasites is based on the trophozoites techniques ac-

cording to Saliba and Kirk (1999) and, due to the semi-asynchronous growth of *P. berghei*, some of the parasites might have been lost during the process. Saponin lysis as a means of parasite isolation was used because of the ease and success of the protocol. Sapogenin, the active compound in saponin, irreversibly permeates the lipid bilayer of RBCs (Baumann *et al.*, 2000). As a wash step, whole blood with CPDA solution, collected from euthanized rats, was diluted with culture medium (CM) and centrifuged ($750 \times g$, 7 min) and supernatant removed. Washed whole blood was resuspended in CM and 5% saponin was added to a final concentration of 0.05% saponin. After the addition of saponin, the mixture is inverted for less than 30 seconds until the colour of the suspended blood turns from red to black whereafter it is immediately centrifuged at $1700 \times g$ for 7 minutes and the supernatant pipetted out. The aliquot was resuspended in CM and centrifuged ($1300 \times g$, 7 min) as a wash step. Glucose-free wash buffer was used to resuspend the aliquots of the solutions, after the CM containing supernatant was pipetted out and centrifuged (6500 RPM, 5 minutes, MSE Micro centaur centrifuge). The isolated parasites were then either stored at -80°C for later lysis or immediately lysed using three freeze-thaw cycles (liquid nitrogen) with intermittent sonification (30 seconds). The lysed parasites were then centrifuged ($13\ 000 \times g$) and the supernatant, containing the glycolytic enzymes, stored at -80°C to be used for the kinetic studies.

3.2.3 Protein concentration determination

The protein concentration of each lysate was measured using Bradford's reagent (Bradford, 1976). In a 96 well plate, $10\ \mu\text{l}$ of series of parasite lysate extract dilutions or bovine serum albumin (0 - 1 mg/ml) was added to $190\ \mu\text{l}$ of filtered Bradford's reagent. The plate was incubated away from direct light for 15 minutes before the absorbance (595 nm) was measured using a spectrophotometer (BioTek PowerWave 340).

3.2.4 Characterizing glycolytic enzymes

The isolated glycolytic enzymes were measured in terms of their maximal velocities at a specific substrate concentration. To measure the velocities, the rates of oxidation and reduction of secondary metabolites, NAD(P)^+ and NAD(P)H , were measured by observing the change in absorbance (340 nm) using a spectrophotometer (BioTek PowerWave 340). All enzymes that did not directly reduce or oxidise the secondary metabolites, were linked to reactions that do by adding linking enzymes (final concentration of 5 U/ml).

3.2.4.1 Hexokinase

The forward reaction velocity of HK was measured by linking the production of G6P to the reduction of NADP^+ (0.8 mM) through G6PDH as linking enzyme. Characterization of the enzyme was done by varying the substrate, Glu (0 - 10 mM) and ATP (0 - 4mM) concentrations and varying the product, ADP (0 - 10 mM), concentration. During each experiment, a constant concentration for each of the metabolites not varied, Glu (10 mM), ATP (2 mM), G6P (0 mM) and ADP (0 mM), was used. Inhibition by G6P (0 - 10 mM) was measuring by linking the

production of ADP to the oxidation of NADH through PK and LDH with PEP (2 mM).

3.2.4.2 Glucosephosphate isomerase

Both the forward and the reverse reaction velocities of GPI were measured. Production of F6P was characterized by varying the substrate, G6P (0 - 10 mM), and measuring the oxidation rate of NADH (0.8 mM) by α -glycerol phosphate dehydrogenase (α -GlyPDH) with ALD, TPI and PFK as linking enzymes. The reverse reaction was characterized by varying product of GPI, F6P (0 - 2 mM), and measure the reduction NADP⁺ (0.8 mM) by G6PDH.

3.2.4.3 Phosphofructokinase

The velocities for the forward and inhibition of the forward reaction were measured as the reaction is irreversible. For all experiments, except for the measurement of the influence of ATP, the ATP was kept constant at a concentration of 1.25 mM. Specific activity of the forward reaction was measured by varying F6P (0 - 10 mM) and varying the ATP (0 - 4 mM) while using a F6P concentration of 0.5 mM and 1 mM. The inhibition of PFK was measured by varying the F16BP (0 - 10 mM) concentration whilst keeping F6P constant at 10 mM. Furthermore, the extent of inhibition of ADP (0 - 2 mM) was measured by using a F6P concentration of 0.5 mM and 1mM. The reaction for the variation for F16BP and ADP included NADH (0.8 mM), LDH, PK and PEP (2 mM) as linking metabolites and enzymes while the reactions that relied on the variation of F6P and ATP included NADH (0.8 mM), α GlyPDH, ALD and TPI as the linking enzymes and metabolites.

3.2.4.4 Aldolase

Specific activity for ALD was only measured in the forward reaction because no reverse linking reaction has been identified as PFK is irreversible. The reaction rates were measured by varying the concentration of F16BP (0 - 1 mM). The linking enzymes included α GlyPDH and TPI. NADH (0.8 mM) served as the linking metabolite.

3.2.4.5 Triosephosphate isomerase

The forward reaction of GAPDH could not be achieved, consequently, only the specific activity for the reverse direction of TPI could be measured by varying the GAP (0 - 0.8 mM) concentration. α GlyPDH served as the linking enzyme along with NADH (0.8 mM).

3.2.4.6 Glyceraldehyde 3-phosphate dehydrogenase

Only the reverse reaction of GAPDH could be measured due to either error in experimental design or reasons unknown to this researcher. Since B13PG is chemically unstable, the velocity was measured by varying 3PG (0 - 2.5 mM) concentration whilst keeping the NADH (0.8 mM) concentration constant and varying NADH (0 -

0.4 mM) concentration whilst keeping the 3PG concentration constant at 5 mM. For both the reactions, PGK is added to convert 3PG to B13PG (complete conversion is assumed).

3.2.4.7 Phosphoglycerate kinase

The specific activity of PGK's reverse reaction is measured by varying the two substrates, 3PG (0 - 2.5 mM) and ATP (0 - 5 mM), concentrations linked to the oxidation of NADH (0.8 mM) through GAPDH as a linking enzyme. The extent of inhibition of ADP (0 - 4 mM) was also measured by varying the ADP concentration. For all the experiments, the reverse metabolites, 3PG (10 mM) and ATP (5 mM), were kept constant unless being the subject of the experiment. The forward reaction could not be measured enzymatically since one of the linking enzymes, PK, also uses ADP as a substrate.

3.2.4.8 Phosphoglycerate mutase

The forward velocity of PGM was measured by varying the substrate, 3PG (0 - 10 mM), concentration and linking the creation of 2PG to the oxidation of NADH (0.8 mM) via LDH along with PK and ENO as linking enzymes and ADP (2 mM) as linking enzyme. For both PGM and ENO, the reverse reaction could not be measured, even at saturation concentrations to be used as a positive control. The reason for the inability to measure the reverse reactions is unknown to this researcher.

3.2.4.9 Enolase

The forward velocity of ENO was measured by varying the substrate, 2PG (0 - 5 mM), concentration and linking the creation of PEP to the oxidation of NADH (0.8 mM) via LDH along with PK as linking enzyme and ADP (2 mM) as linking enzyme.

3.2.4.10 Pyruvate kinase

Specific activity of PK was only measured in the forward reaction, due to the irreversible nature of PK, by varying the concentration of the substrates, ADP (0 - 2.5 mM) and PEP (0 - 4 mM), and linking the creation of Pyr to the oxidation of NADH (0.8 mM) via LDH. The extent of PK's forward inhibition was measured by varying the concentration of the inhibitors, ATP (0 - 4 mM) and Pyr (0 - 100 mM). For the forward reactions, ADP measurements by using a PEP concentration of 5 mM and PEP measurements were done by using a ADP concentration of 0.5 mM and 2.5 mM. Inhibition by ATP was measured by using an ADP concentration of 0.5 mM and PEP concentration of 1.25 mM and 2.5 mM. Pyruvate inhibition was measured by using a ADP concentration of 1 mM and PEP concentration of 1.25 mM with LDH as linking enzyme.

3.2.4.11 Lactate Dehydrogenase

LDH was characterised in both directions. The forward reaction velocity was measured by varying the substrate, Pyr (0 - 2 mM) and NADH (0 - 0.4 mM), concen-

trations. The accompanying substrate was kept constant, which included Pyr (2.5 mM) during the NADH testing and NADH (0.8 mM) during the Pyr testing. The velocities of the reverse direction were measured by varying the products, Lac (0 - 10 mM) and NAD^+ (0 - 1 mM), while keeping the accompanying product, Lac (20 mM) and NAD^+ (2 mM), constant. No linking enzymes or metabolites were used during LDH characterization.

3.2.5 Computational Analysis and Statistics

Data obtained from the spectrophotometer was interpreted with GraphPad Prism 5.0 to obtain the maximal activity of each reaction which was normalised with the extract protein concentration to produce the specific activity. The specific activity of each reaction was in turn imported into Mathematica version 10.0 to produce graphs and fitted lines, as well as the kinetic parameters and SEM.

3.3 Results and Discussion

Very promising results were obtained for the kinetic study, showing many similarities to the work done on *P. falciparum*. Every data point was measured in technical triplicates and the standard error of means (SEM) for technical replicates of the different data points is omitted as the SEM was negligibly small (fall within the symbol size) in the vast majority of the data points. Four data points were obtained per experiment, but the limited available biomass obtained from the successful isolation, forced prioritizing of certain enzyme characterizations. Here follows the results obtained from the enzyme assays and the subsequent rate equations fittings.

3.3.1 Hexokinase

The first reaction characterised is that of HK. HK, the first enzyme of glycolysis and catalyses the first reaction reaction in the glycolytic model (figure 3.1), converting glucose and Mg-ATP-complex to G6P, Mg-ADP-complex and H^+ . With the assumption that the reaction is irreversible due to the large K_{eq} from literature, the enzyme was characterised for the forward reaction in terms of glucose and ATP as its substrates and ADP and G6P as the enzymes inhibitory products. Figure 3.2 shows the data obtained from the kinetic study with the velocity of the reaction plotted against the concentration of the substrate or product. The glucose saturation curve is not clear from the data points obtained, but the product inhibition from ADP and G6P follow normal Michaelis-Menten curves. ATP appears to inhibit the reaction above a certain concentration, similar to results obtained from Kumar and Banyal (1996), suggesting that hexokinase is sensitive to substrate inhibition by ATP; consequently, substrate inhibition was then added to the equation. A Michaelis-Menten equation (eq 3.5) with substrate inhibition and replacement of the V_{max} for the reverse, by using the Haldane relation, reaction was then plotted to the data points, represented by the curves in 3.2. The curves appear to adequately fit the data and the Michaelis-Menten constants along with the V_{max} forward and K_{eq} , from literature, is displayed in table 3.1. The kinetic parameters show good agreement to the work of Penkler *et al.* (2015) on *P. falciparum*, shown in table 3.1.

$$v_{HK} = \frac{\frac{\text{atp} \cdot \text{glu} \cdot V_f}{K_{\text{atp}} \cdot K_{\text{glu}}} - \frac{\text{adp} \cdot \text{g6p} \cdot V_f}{K_{\text{atp}} \cdot K_{\text{eq}} \cdot K_{\text{glu}}}}{\left(\frac{\text{atp}}{K_{\text{iatp}}} + 1\right) \left(\frac{\text{adp}}{K_{\text{adp}}} + \frac{\text{atp}}{K_{\text{atp}}} + 1\right) \left(\frac{\text{g6p}}{K_{\text{g6p}}} + \frac{\text{glu}}{K_{\text{glu}}} + 1\right)} \quad (3.5)$$

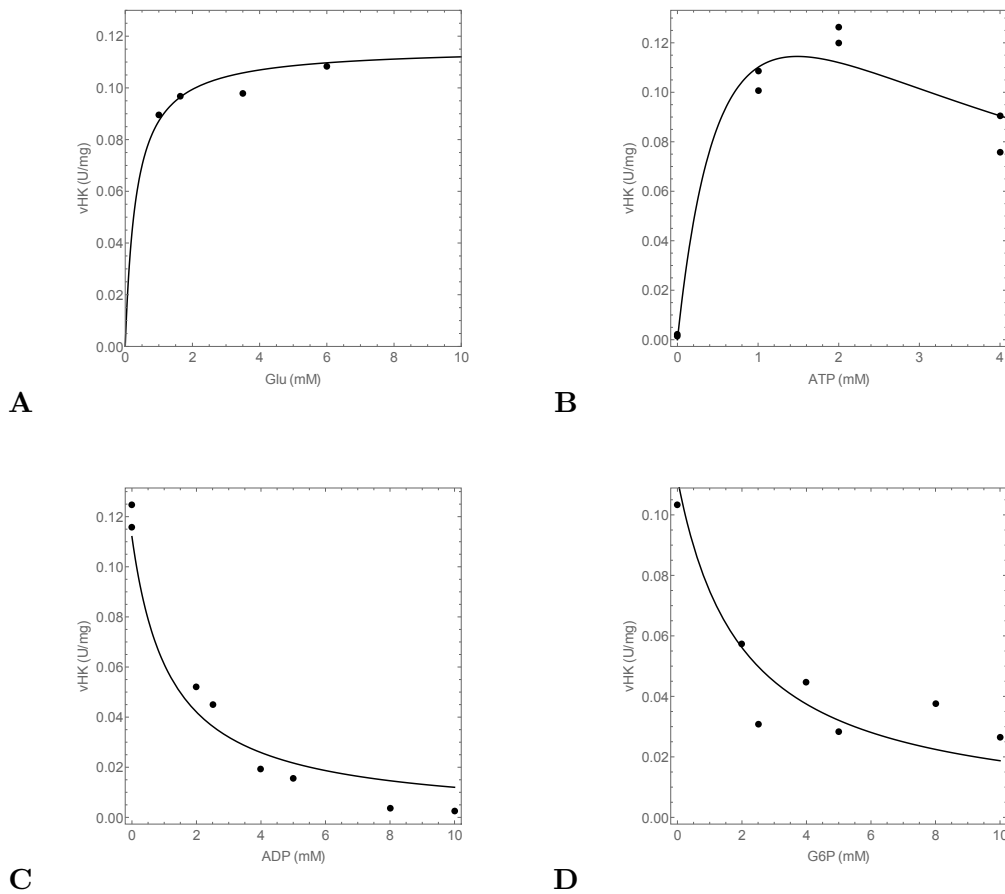


Figure 3.2: Results from the kinetic characterization and subsequent equation fitting of *P. berghei* hexokinase. The velocities of the forward reaction of HK in terms of the substrates, (A) Glu and (B) ATP, are shown with the inhibition of the products, (C) ADP and (D) G6P. Equation 3.5 is fitted to the data set to produce the fitted lines that describe the data well (adjusted $R^2 = 0.98$).

3.3.2 Glucosephosphate isomerase

The reversible conversion of G6P to F6P is mediated by GPI and is the second step in glycolysis. The kinetic parameters of the enzyme were characterised by varying the substrate concentration and measuring the velocity of F6P production and by varying the product concentration and measuring the velocity of G6P creation. Data

Table 3.1: Enzyme kinetic parameters for *P. berghei* HK. The Michaelis constants for the different metabolites and the maximal velocity of the forward reaction that were fitted using the data in figure 3.2 and equation 3.5 are displayed in the table alongside the values Penkler *et al.* (2015) fitted or used for *P. falciparum*. The asymptotic standard error is given with all the fitted values.

Parameter	Fitted Value	Literature value
V_f ($\mu\text{mol}\cdot\text{min}^{-1}\cdot\text{mg}^{-1}$)	0.47 ± 0.02	0.39 ± 0.09
K_{glu} (mM)	0.33 ± 0.15	0.17 ± 0.02
K_{atp} (mM)	1.50 ± 0.22	0.7 ± 0.03
K_{g6p} (mM)	0.06 ± 0.03	0.04 ± 0.01
K_{adp} (mM)	0.33 ± 0.15	0.8 ± 0.1
K_{eq} (mM)	-	1310

obtained from the kinetic study is displayed on figure 3.3 A and B. Substrate inhibition was observed at higher concentration, above 2.5 mM, of G6P. Using a random order uni-uni Michaelis-Menten equation (eq 3.6) with substrate inhibition factor, the fitted curves on figure 3.3 A and B was obtained. Table 3.2 presents the values for the maximal velocities, both forward and reverse, the Michaelis-Menten constants for the reaction and the K_{eq} that was calculated using the Haldane relation. All the kinetic parameters fitted well ($p < 0.01$), except for K_{f6p} . No literature on substrate inhibition of G6P could be found to date. The substrate inhibition could be due to inhibition by 6-phosphogluconate (Parr, 1956). According to Carter (1970), *P. berghei* produces 6-phosphogluconate dehydrogenase as a means to create NADPH for combating oxidative stress via the pentose phosphate pathway. Since no NADPH is added to the assay the reaction is unlikely. Further investigation is needed to elucidate the cause of the substrate inhibition.

$$v_{GPI} = \frac{\frac{g6p \cdot V_f}{K_{g6p}} - \frac{f6p \cdot V_r}{K_{f6p}}}{\left(\frac{g6p}{K_{g6p}} + 1\right) \left(\frac{f6p}{K_{f6p}} + \frac{g6p}{K_{g6p}} + 1\right)} \quad (3.6)$$

Table 3.2: Enzyme kinetic parameters for *P. berghei* GPI. The Michaelis constants for the different metabolites and the maximal velocities of the forward reaction and reverse direction that were fitted using the data in figure 3.3 and equation 3.6 are displayed in the table alongside the values Penkler *et al.* (2015) fitted or used for *P. falciparum*. The asymptotic standard error is given with all the fitted values.

Parameter	Fitted Value	Literature value
V_f ($\mu\text{mol}\cdot\text{min}^{-1}\cdot\text{mg}^{-1}$)	1.77 ± 0.16	3.7 ± 0.02
V_r ($\mu\text{mol}\cdot\text{min}^{-1}\cdot\text{mg}^{-1}$)	0.29 ± 0.07	1.4 ± 0.03
K_{g6p} (mM)	2.06 ± 0.53	1.0 ± 0.1
K_{f6p} (mM)	0.19 ± 0.17	0.10 ± 0.01
K_{eq} (mM)	0.55	0.3 ± 0.1

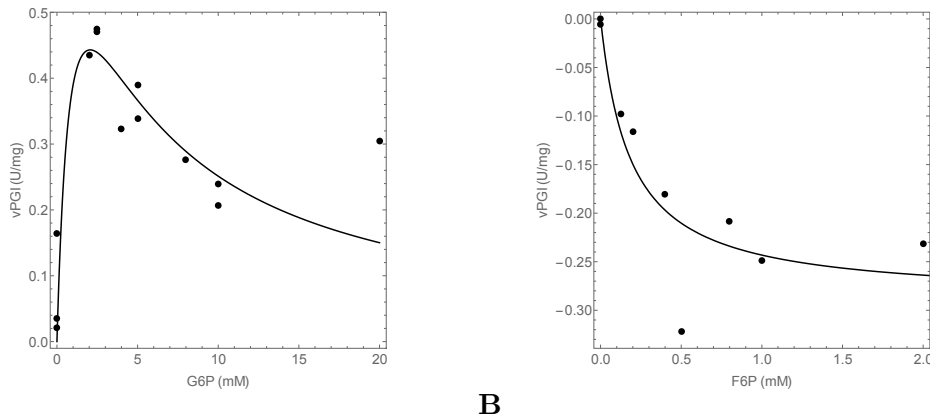


Figure 3.3: Results from the kinetic characterization and subsequent equation fitting of *P. berghei* phosphoglucose isomerase. The velocities of the forward (A) and reverse (B) reactions of the enzymes are displayed by altering the concentration of the substrate, G6P, and product, F6P, respectively. Equation 3.6 is fitted to the data set to produce the fitted lines that describe the data well (adjusted $R^2 = 0.94$).

3.3.3 Phosphofructokinase

Phosphofructokinase is a key-regulatory enzyme in the glycolytic pathway and catalyses the conversion of F6P and ATP to F16BP and ADP. Figure 3.4 shows the results of the kinetic experiments performed on PFK. The problems with reproducibility of the experiment, availability of *P. berghei* extract and human error allowed for only one experiment to be performed for two different concentrations of F6P. Since PFK shows substrate inhibition for ATP and product inhibition, two different concentrations of F6P was used for the characterization of the binding of the primary metabolites. Equation 3.7 was used to plot the fitted lines on figure 3.4. The fitted lines describe the data adequately, but more data points are needed to produce a better fit. The combined work of Buckwitz et Al (1990a, 1990b and 1988) used Hill's coefficient to describe the effect the homo-oligomer nature of PFK had on the activation and inhibition of the various metabolites reacting with PFK. Future work on the model necessitates investigation into the possible of use of Hill's coefficient to describe the data. Michaelis-Menten constants and the maximal forward velocity of the reaction is displayed in Table 3.3 alongside the values Penkler (2009) obtained in his M.Sc thesis. The characterization of PFK needs to be repeated and Hill's coefficient applied to the equations to present a more adequate representation of the kinetic parameters of PFK.

$$v_{PFK} = \frac{atp \cdot f6p \cdot Vf}{K_{atp} \cdot K_{f6p} \left(\frac{atp}{K_{atp}} + 1 \right) \left(\frac{adp}{K_{adp}} + \frac{atp}{K_{atp}} + 1 \right) \left(\frac{f16bp}{K_{f16bp}} + \frac{f6p}{K_{f6p}} + 1 \right)} \quad (3.7)$$

Table 3.3: Enzyme kinetic parameters for *P. berghei* PFK. The Michaelis constants for the different metabolites and the maximal velocity of the forward reaction that were fitted using the data in figure 3.4 and equation 3.7 are displayed in the table alongside the values Penkler *et al.* (2015) fitted or used for *P. falciparum*. The asymptotic standard error is given with all the fitted values.

Parameter	Fitted Value	Literature value
V_f ($\mu\text{mol}\cdot\text{min}^{-1}\cdot\text{mg}^{-1}$)	2.1 ± 2.8	1.9 ± 0.3
K_{atp} (mM)	3.6 ± 0.86	0.79 ± 0.04
K_{f6p} (mM)	0.21 ± 0.40	1.07 ± 0.06
K_{f16bp} (mM)	3.2 ± 0.88	3.6 ± 0.5
K_{adp} (mM)	0.09 ± 0.16	0.7 ± 0.1

3.3.4 Aldolase

Aldolase catalyses the aldol cleaving of F16BP into two triose phosphates, namely DHAP and GAP. The forward reaction of the enzyme was characterized by varying the concentration of the substrate, F16BP. Results for the kinetic study is displayed in figure 3.5. Using a random order uni-bi Michaelis-Menten equation (eq 3.8), a line was fitted to the equation which fits the data well. The near irreversible nature of PFK (if used as linking enzyme) did not allow for the reverse characterization of the enzyme and the Haldane relationship with the K_{eq} from Penkler *et al.* (2015), was used. Due to the presence of TPI, the binding coefficients could not be measured for either GAP or DHAP and so K_{GAP} and K_{DHAP} was used from the work of Penkler *et al.* (2015). A summary of the kinetic data obtained is displayed in table 3.4, alongside Penkler's results. A 20 times difference is observed between the two different V_f 's. The low V_f could be due to the low pH of 7.17 (optimal pH of between pH 7.8 and 8.2) or due to degradation over time since it has been observed that 31% of aldolase is destroyed in 24 hours at 4° C (Kumar and Banyal, 1997). The K_{f16bp} obtained closely matches that of Kumar and Banyal (1997) (0.025), but is more than 2-fold lower than the value determined by Penkler *et al.* (2015).

$$v_{ALD} = \frac{f16bp \cdot V_f \cdot \left(1 - \frac{dhap \cdot gap}{f16bp \cdot K_{eq}}\right)}{K_{f16bp} \left(\frac{dhap \cdot gap}{K_{dhap} \cdot K_{gap}} + \frac{dhap}{K_{dhap}} + \frac{f16bp}{K_{f16bp}} + \frac{gap}{K_{gap}} + 1\right)} \quad (3.8)$$

3.3.5 Triosephosphate isomerase

The reversible conversion from DHAP to GAP is catalysed by TPI. The reaction was only characterised in the reverse direction (figure 3.6), as the forward reaction of the linking enzyme, GAPDH, would not react. A uni-uni Michaelis-Menten equation (eq 3.9) with PEP inhibition and Haldane relation to replace the maximal forward velocity was used to plot the line on the graph and calculate the kinetic parameters in table 3.5. The K_{dhap} , K_{ipep} and K_{eq} was used from Penkler *et al.* (2015) as this could not be measured. The reaction occurred without the addition of GAP, which

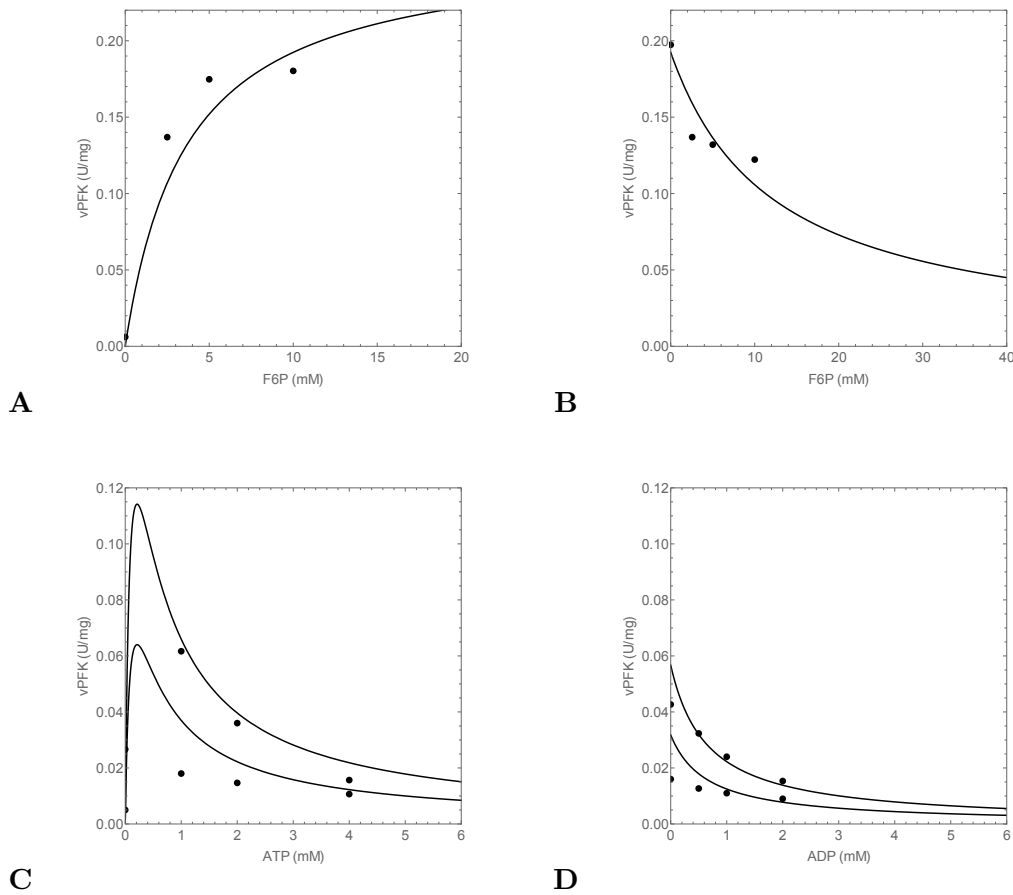


Figure 3.4: Results from the kinetic characterization and subsequent equation fitting of *P. berghei* phosphofructokinase. The velocities of the forward reaction of PFK in terms of the substrates, (A) F6P and (C) ATP, is shown with the inhibition by the products, (B) F16BP and (D) ADP. Equation 3.7 is fitted to the data set to produce the fitted lines that adequately describe (adjusted $R^2 = 0.97$).

negatively influences the accuracy of the parameter fitting.

$$v_{TPI} = \frac{\frac{dhap \cdot K_{eq} \cdot V_r}{K_{gap}} - \frac{gap \cdot V_r}{K_{gap}}}{\frac{dhap}{K_{dhap}} + \frac{gap}{K_{gap}}} \quad (3.9)$$

3.3.6 Glyceraldehyde 3-phosphate dehydrogenase

The sixth step in the central carbon metabolism is the conversion of GAP, NAD^+ and inorganic phosphate to B13PG and NADH which is catalysed by glyceraldehyde-3-phosphate dehydrogenase. GAPDH was only characterised (figure 3.7) in the reverse direction for both enzyme products, (A) B13PG and (B) NADH, as the forward reaction could not be measured. Time constraints did not allow further investigation as to the exact reason why the forward reaction could not be measured.

Table 3.4: Enzyme kinetic parameters for *P. berghei* ALD. The Michaelis constants for the different metabolites and the maximal velocity of the forward reaction that were fitted using the data in figure 3.5 and equation 3.8 are displayed in the table alongside the values Penkler *et al.* (2015) fitted or used for *P. falciparum*. The asymptotic standard error is given with all the fitted values.

Parameter	Fitted Value	Literature value
V_f ($\mu\text{mol}\cdot\text{min}^{-1}\cdot\text{mg}^{-1}$)	0.013 ± 0.0008	0.27 ± 0.01
K_{f16bp} (mM)	0.029 ± 0.013	0.068 ± 0.004
K_{gap} (mM)	-	0.05 ± 0.02
K_{dhap} (mM)	-	0.11 ± 0.09
K_{eq} (mM)	-	0.09

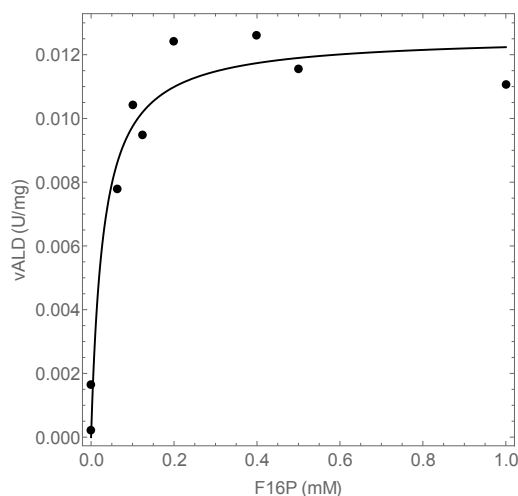


Figure 3.5: Results from the kinetic characterization and subsequent equation fitting of *P. berghei* aldolase. The velocities of the forward reaction of ALD, measured by varying the substrate, F16BP, concentration is shown. Equation 3.8 is fitted to the data set to produce the fitted lines that describe the data well (adjusted $R^2 = 0.99$).

The velocities of the reverse reaction was measured by altering PG3 concentration with the addition of ATP and PGK which was assumed to be readily converted back into B13PG due to PGK's high K_{eq} . Using a random order bi-bi Michaelis-Menten equation (eq 3.10) in combination with the Haldane relation, lines were fitted to the data set that described the data well. Kinetic parameters for the characterization are displayed in table 3.6. The maximal velocity of the reverse reaction is 10 times lower than the velocity obtained by Penkler *et al.* (2015) for *P. falciparum* and the binding coefficient for B13PG is 20 times greater, necessitating investigation into

Table 3.5: Enzyme kinetic parameters for *P. berghei* TPI. The Michaelis constants for the different metabolites and the maximal velocity of the reverse reaction that were fitted using the data in figure 3.6 and equation 3.9 are displayed in the table alongside the values Penkler *et al.* (2015) fitted or used for *P. falciparum*. The asymptotic standard error is given with all the fitted values.

Parameter	Fitted Value	Literature value
V_r ($\mu\text{mol}\cdot\text{min}^{-1}\cdot\text{mg}^{-1}$)	5.1 ± 3.6	15 ± 1
K_{gap} (mM)	0.50 ± 0.72	0.34 ± 0.04
K_{dhap} (mM)	-	2.0 ± 0.3
K_{ipep} (mM)	-	0.016 ± 0.002
K_{eq} (mM)	-	0.08 ± 0.03

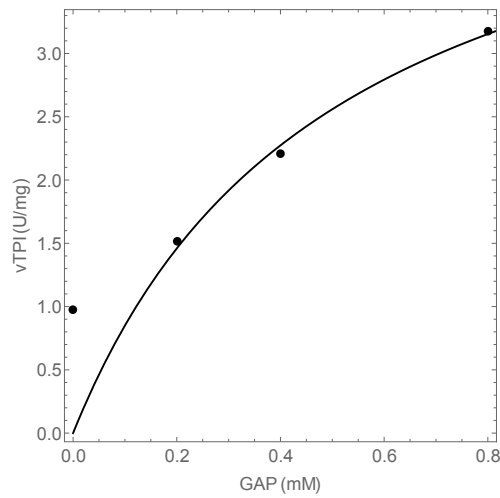


Figure 3.6: Results from the kinetic characterization and subsequent equation fitting of *P. berghei* triosephosphate isomerase. The velocities of the reverse reaction of TPI, measured by varying the enzyme product, GAP, concentration are shown. Equation 3.9 is fitted to the data set to produce the fitted lines that does not describe the data well (adjusted $R^2 = 0.90$).

the reason for the large difference.

$$v_{GAPDH} = \frac{\frac{\text{gap}\cdot\text{Keq}\cdot\text{nad}\cdot\text{Vr}}{\text{Kb13pg}\cdot\text{Knadh}} - \frac{\text{b13pg}\cdot\text{nadh}\cdot\text{Vr}}{\text{Kb13pg}\cdot\text{Knadh}}}{\left(\frac{\text{b13pg}}{\text{Kb13pg}} + \frac{\text{gap}}{\text{Kgap}} + 1\right) \left(\frac{\text{nad}}{\text{Knad}} + \frac{\text{nadh}}{\text{Knadh}} + 1\right)} \quad (3.10)$$

3.3.7 Phosphoglycerate kinase

The conversion of B13PG and ADP to PG3 and ATP is catalysed by the enzyme phosphoglycerate kinase and functions as the first ATP producing step. Charac-

Table 3.6: Enzyme kinetic parameters for *P. berghei* GAPDH. The Michaelis constants for the different metabolites and the maximal velocity of the reverse reaction that were fitted using the data in figure 3.7 and equation 3.10 are displayed in the table alongside the values Penkler *et al.* (2015) fitted or used for *P. falciparum*. The asymptotic standard error is given with all the fitted values.

Parameter	Fitted Value	Literature value
V_r ($\mu\text{mol}\cdot\text{min}^{-1}\cdot\text{mg}^{-1}$)	0.14 ± 0.009	1.2 ± 0.3
K_{gap} (mM)	-	0.9 ± 0.1
K_{b13pg} (mM)	0.55 ± 0.11	0.024 ± 0.002
K_{nad} (mM)	-	0.57 ± 0.06
K_{nadh} (mM)	0.011 ± 0.005	0.029 ± 0.004
K_{eq} (mM)	-	0.0035

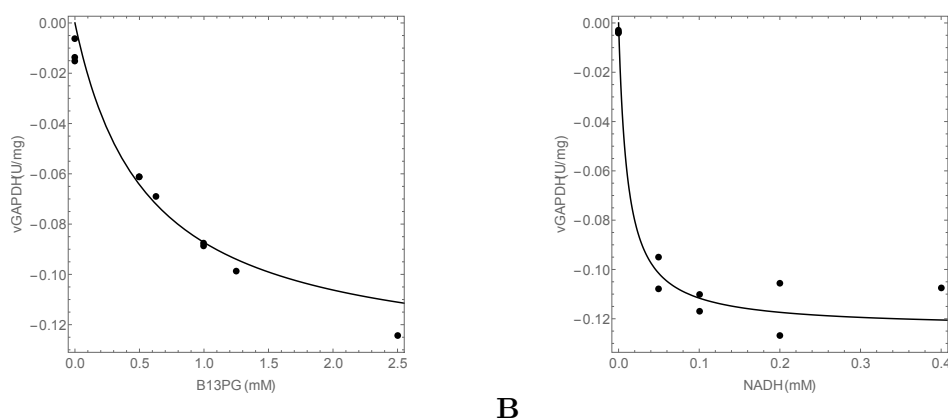


Figure 3.7: Results from the kinetic characterization and subsequent equation fitting of *P. berghei* glyceraldehyde 3-phosphate dehydrogenase. The velocities of the reverse reactions of GAPDH, measured by varying the enzyme products, (A) B13PG and (B) NADH, concentrations is shown. Equation 3.10 is fitted to the data set to produce the fitted lines that describes the data well (adjusted $R^2 = 0.99$).

terization of PGK was only possible in the reverse direction by measuring GAPDH activity, because the ADP is a substrate of one of the possible forward linking enzymes, PK, and B13PG is unstable. Figure 3.8 shows the results of the kinetic study done on PGK for both the enzyme's products, ATP and PG3, as well as inhibition by the substrate ADP. A random order bi-bi Michaelis-Menten equation (eq 3.11), along with the Haldane relation to compensate for the inability to measure the forward reaction, was fitted to the data set to produce the fitted lines that describe the data well. The Michaelis constants and maximal velocities of the fitted lines are presented in table 3.7. Due to inability to achieve a forward reaction for GAPDH, K_{B13PG} for PGK could not be measured and instead was used from the work of

Penkler *et al.* (2015).

$$vPGK = \frac{\text{atp} \cdot \text{pg3} \cdot V_r \left(\frac{\text{adp} \cdot \text{b13pg} \cdot K_{eq}}{\text{atp} \cdot \text{pg3}} - 1 \right)}{K_{atp} \cdot K_{pg3} \left(\frac{\text{adp}}{K_{adp}} + \frac{\text{atp}}{K_{atp}} + 1 \right) \left(\frac{\text{b13pg}}{K_{b13pg}} + \frac{\text{pg3}}{K_{pg3}} + 1 \right)} \quad (3.11)$$

Table 3.7: Enzyme kinetic parameters for *P. berghei* PGK. The Michaelis constants for the different metabolites and the maximal velocity of the reverse reaction that were fitted using the data in figure 3.8 and equation 3.11 are displayed in the table alongside the values Penkler *et al.* (2015) fitted or used for *P. falciparum*. The asymptotic standard error is given with all the fitted values.

Parameter	Fitted Value	Literature value
V_r ($\mu\text{mol} \cdot \text{min}^{-1} \cdot \text{mg}^{-1}$)	0.64 ± 0.03	0.39 ± 0.09
K_{adp} (mM)	0.33 ± 0.15	0.15 ± 0.01
K_{atp} (mM)	1.02 ± 0.17	0.77 ± 0.05
K_{3pg} (mM)	1.42 ± 0.14	0.27 ± 0.02
K_{b13pg} (mM)	-	0.013
K_{eq} (mM)	-	3200

3.3.8 Phosphoglycerate mutase

The reversible interconversion of PG3 to PG2 is catalysed by phosphoglycerate mutase. Only the forward reaction could be characterized for PGM. Exact reason for the inability to measure the forward reaction could not be determined during the experimental phase of the project and requires further investigation. The data obtained from the kinetic study is displayed on figure 3.9 and the lines describe the data very well. The fitted lines on the figure were produced by applying a uni-uni Michaelis-Menten equation along with the Haldane relations to compensate for the reverse reaction to the data set. Kinetic parameters for the fitted equation (eq 3.12) are presented in table 3.8. Since the reverse reaction could not be measured, the K_{pg2} and K_{eq} was used from the work of Penkler *et al.* (2015).

$$vPGM = \frac{\frac{\text{pg3} \cdot V_f}{K_{pg3}} - \frac{\text{pg2} \cdot V_f}{K_{eq} \cdot K_{pg3}}}{\frac{\text{pg2}}{K_{pg2}} + \frac{\text{pg3}}{K_{pg3}} + 1} \quad (3.12)$$

3.3.9 Enolase

The metalloenzyme, enolase, is responsible for catalysing the interconversion of PG2 and PEP. Similar to PGM, only the forward reaction could be kinetically measured and the results of the kinetic experiments for ENO are presented in figure 3.10. Using a uni-uni Michaelis-Menten equation, along with the Haldane relation to replace the maximal velocity of the reverse reaction, and applying it (eq 3.13) to the data set, the fitted lines were produced which describe the data well. the kinetic parameters

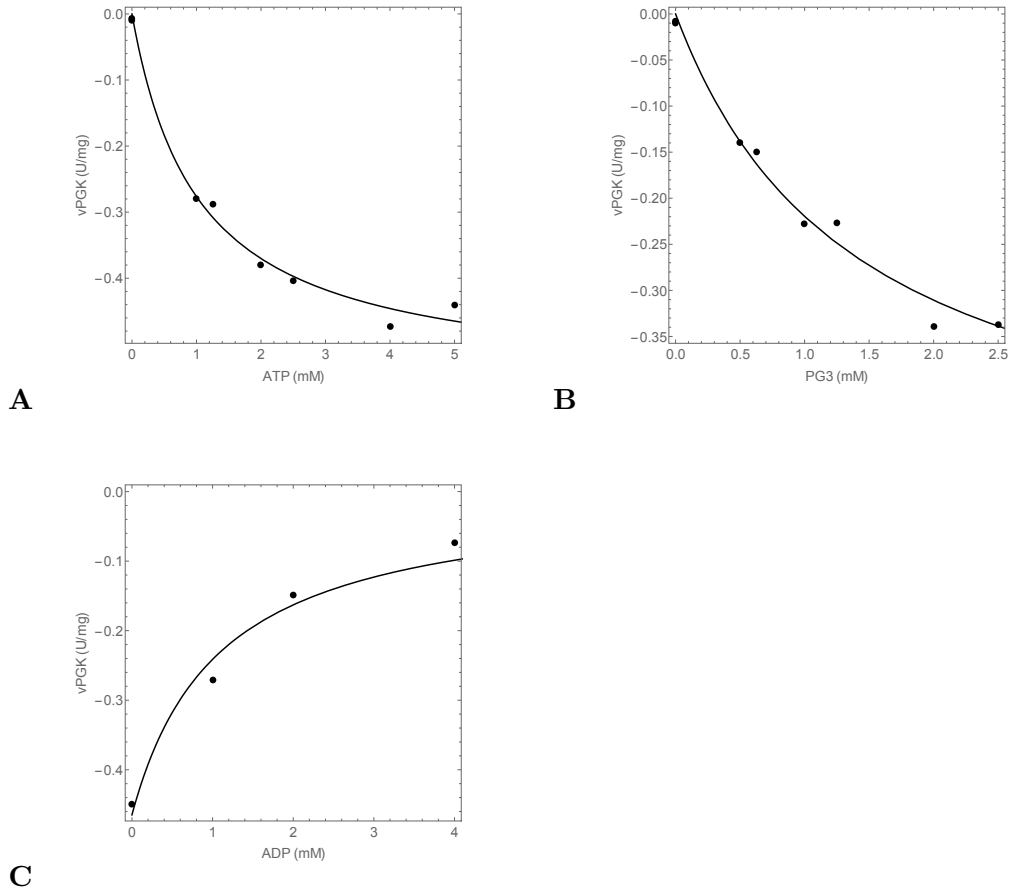


Figure 3.8: Results from the kinetic characterization and subsequent equation fitting of *P. berghei* phosphoglycerate kinase. The velocities of the reverse reactions of PGK, measured by varying the enzyme products, (A) ATP and (B) PG3, concentrations with inhibition of the enzyme substrate, (C) ADP, are shown. Equation 3.11 is fitted to the data set to produce the fitted lines that describes the data well (adjusted $R^2 = 1.00$).

for the fitted lines are displayed in table 3.9. The lack of characterization of the reverse reaction led to the use of the K_{pep} and K_{eq} from Penkler *et al.* (2015). It should also be noted that the excessive Mg^{2+} concentration, which is known to inhibit the reaction, could have caused at least 20% inhibition at concentration of 10 mM and that the kinetic measurements were done at a pH lower than that of the ideal pH (7.4 to 7.6), but rather at a physiological pH of 7.17 (Pal-Bhowmick *et al.*, 2004).

$$v_{ENO} = \frac{\frac{pg2 \cdot V_f}{K_{pg2}} - \frac{pep \cdot V_f}{K_{eq} \cdot K_{pg2}}}{\frac{pep}{K_{pep}} + \frac{pg2}{K_{pg2}} + 1} \quad (3.13)$$

Table 3.8: Enzyme kinetic parameters for *P. berghei* PGM. The Michaelis constants for the different metabolites and the maximal velocity of the forward reaction that were fitted using the data in figure 3.9 and equation 3.12 are displayed in the table alongside the values Penkler *et al.* (2015) fitted or used for *P. falciparum*. The asymptotic standard error is given with all the fitted values.

Parameter	Fitted Value	Literature value
V_f ($\mu\text{mol}\cdot\text{min}^{-1}\cdot\text{mg}^{-1}$)	0.25 ± 0.01	0.87 ± 0.09
K_{pg2} (mM)	-	0.32 ± 0.02
K_{pg3} (mM)	3.0 ± 0.44	1.7 ± 0.1
K_{eq} (mM)	-	0.30

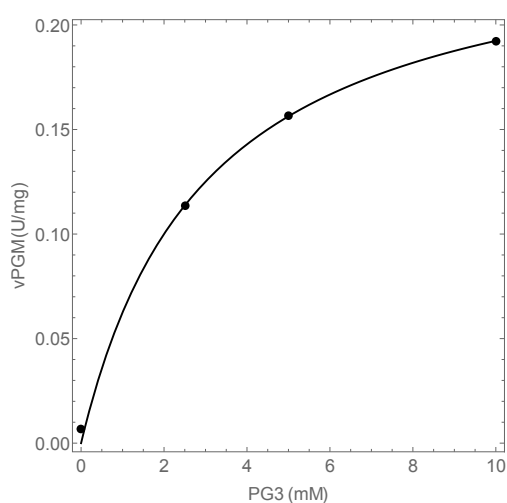


Figure 3.9: Results from the kinetic characterization and subsequent equation fitting of *P. berghei* PGM. The velocities of the forward reaction of PGM, measured by varying the enzyme substrate, PG3, concentration are shown. Equation 3.12 is fitted to the data set to produce the fitted lines that describe the data well (adjusted $R^2 = 1.00$).

3.3.10 Pyruvate kinase

The second ATP yielding reaction is the conversion of PEP and ADP to Pyr and ATP, catalysed by the enzyme pyruvate kinase with a magnesium ion as cofactor. The reaction is assumed to be irreversible due to the large difference in free energy (Emmerling *et al.*, 2002). PK was characterised in the forward direction (figure 3.11) by varying the two substrates, PEP and ADP, and the inhibition by the products, ATP and Pyr, was also measured with a LDH linked assay. Since PK is a morphoein protein and subject to allosteric regulation, the MWC equation was used with an irreversible bi-substrate Michaelis-Menten equation (eqns 3.14 and 3.15) to plot the fitted lines on the graphs. The fitted lines do not adequately describe the data obtained from the kinetic experiments. Additional data points are needed for

Table 3.9: Enzyme kinetic parameters for *P. berghei* ENO. The Michaelis constants for the different metabolites and the maximal velocity of the forward reaction that were fitted using the data in figure 3.10 and equation 3.13 are displayed in the table alongside the values Penkler *et al.* (2015) fitted or used for *P. falciparum*. The asymptotic standard error is given with all the fitted values.

Parameter	Fitted Value	Literature value
V_f ($\mu\text{mol}\cdot\text{min}^{-1}\cdot\text{mg}^{-1}$)	0.56 ± 0.06	1.3 ± 0.4
K_{pg2} (mM)	0.62 ± 0.30	0.52 ± 0.04
K_{pep} (mM)	-	1.3 ± 0.1
K_{eq} (mM)	-	5.7

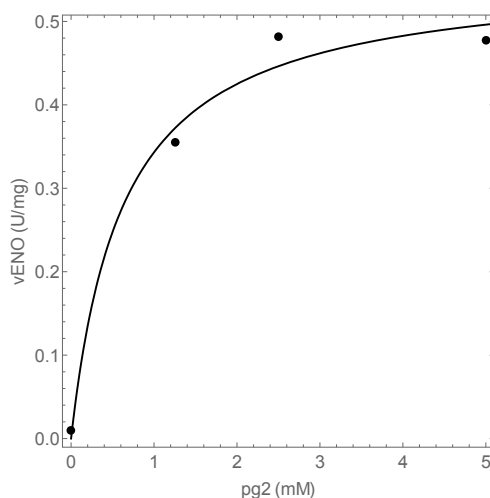


Figure 3.10: Results from the kinetic characterization and subsequent equation fitting of *P. berghei* enolase. The velocities of the forward reaction of ENO, measured by varying the enzyme substrate, PG2, concentration are shown. Equation 3.13 is fitted to the data set to produce the fitted lines that describe the data well (adjusted $R^2 = 0.99$).

greater accuracy. A summary of the kinetic parameters, which includes the Michaelis constants, V_{max} for the forward reaction and the MWC parameters is given in table 3.10. The substrate binding sites, labeled “n” in the equations and fitted values represents the number of allosteric binding sites and was used from the work of Penkler *et al.* (2015). Significant difference exist between the fitted values for *P. berghei* and *P. falciparum*, from the work of Penkler *et al.* (2015), which is evident when looking at goodness of fit of the curves to the data points, necessitating repeats for better results.

$$vPK = \frac{\text{adp} \cdot \text{pep} \cdot V_f}{K_{\text{adp}} \cdot K_{\text{pep}}(L + 1) \left(\frac{\text{adp}}{K_{\text{adp}}} + 1 \right) \left(\frac{\text{pep}}{K_{\text{pep}}} + 1 \right)} \quad (3.14)$$

$$L = L_0 \left(\left(\frac{\text{adp}}{K_{i\text{adp}}} + \frac{\text{atp}}{K_{i\text{atp}}} \right)^n + 1 \right) \left(\left(\frac{\text{pep}}{K_{i\text{pep}}} + \frac{\text{pyr}}{K_{i\text{pyr}}} \right)^n + 1 \right) \quad (3.15)$$

Table 3.10: Enzyme kinetic parameters for *P. berghei* PK. The Michaelis constants for the different metabolites, the maximal velocity of the forward reaction and the Monod-Wyman-Changeux elements that were fitted using the data in figure 3.11 and equations 3.14 and 3.15 are displayed in the table alongside the values Penkler *et al.* (2015) fitted or used for *P. falciparum*. The asymptotic standard error is given with all the fitted values.

Parameter	Fitted Value	Literature value
V_f ($\mu\text{mol}\cdot\text{min}^{-1}\cdot\text{mg}^{-1}$)	0.36 ± 0.59	2.3
K_{adp} (mM)	0.92 ± 0.82	0.30 ± 0.050
K_{pep} (mM)	0.36 ± 0.53	0.39 ± 0.047
$K_{i\text{pyr}}$ (mM)	3.19 ± 0.56	69 ± 6.7
$K_{i\text{atp}}$ (mM)	3.30 ± 0.54	1.4 ± 0.12
$K_{i\text{adp}}$ (mM)	2.9 ± 1.0	1.9 ± 0.15
$K_{i\text{pep}}$ (mM)	3.30 ± 0.56	2.8 ± 0.24
L_0 (mM)	0.12 ± 0.12	0.20 ± 0.09
n (mM)	4	4

3.3.11 Lactate dehydrogenase

The most complete kinetic characterization was that of the kinetic analysis of the enzyme lactate dehydrogenase which catalyses the conversion of Pyr and NADH to Lac and NAD^+ . Both the velocities of the forward and reverse reaction of the enzyme was measured by varying the concentrations of the substrates and the products whilst keeping the other metabolites constant; data displayed in figure 3.12. The fitted lines were constructed by applying a random order bi-bi Michaelis-Menten equation (eq. 3.16) to the data set which describes the data well. Table 3.11 was constructed from the kinetic parameters of the equation fitting. The majority of the kinetic parameters correlate to the values obtained for *P. falciparum*, from the work of Penkler *et al.* (2015), well, except for the binding coefficient for lac and the K_{eq} , which differ by a few magnitudes.

$$v_{LDH} = \frac{\frac{\text{nadh}\cdot\text{pyr}\cdot V_f}{K_{\text{nadh}}\cdot K_{\text{pyr}}} - \frac{\text{lac}\cdot\text{nad}\cdot V_r}{K_{\text{lac}}\cdot K_{\text{nad}}}}{\left(\frac{\text{lac}}{K_{\text{lac}}} + \frac{\text{pyr}}{K_{\text{pyr}}} + 1 \right) \left(\frac{\text{nad}}{K_{\text{nad}}} + \frac{\text{nadh}}{K_{\text{nadh}}} + 1 \right)} \quad (3.16)$$

3.3.12 Summary

In this chapter we have partially characterized the kinetic parameters of *P. berghei* glycolytic enzymes. The kinetic parameters obtained from the characterization are summarised in table 3.12. The aim of this chapter was to assess the feasibility of characterizing the different glycolytic enzymes and we have proven that this is indeed possible. Some of the enzymes have incomplete characterizations and the parameters

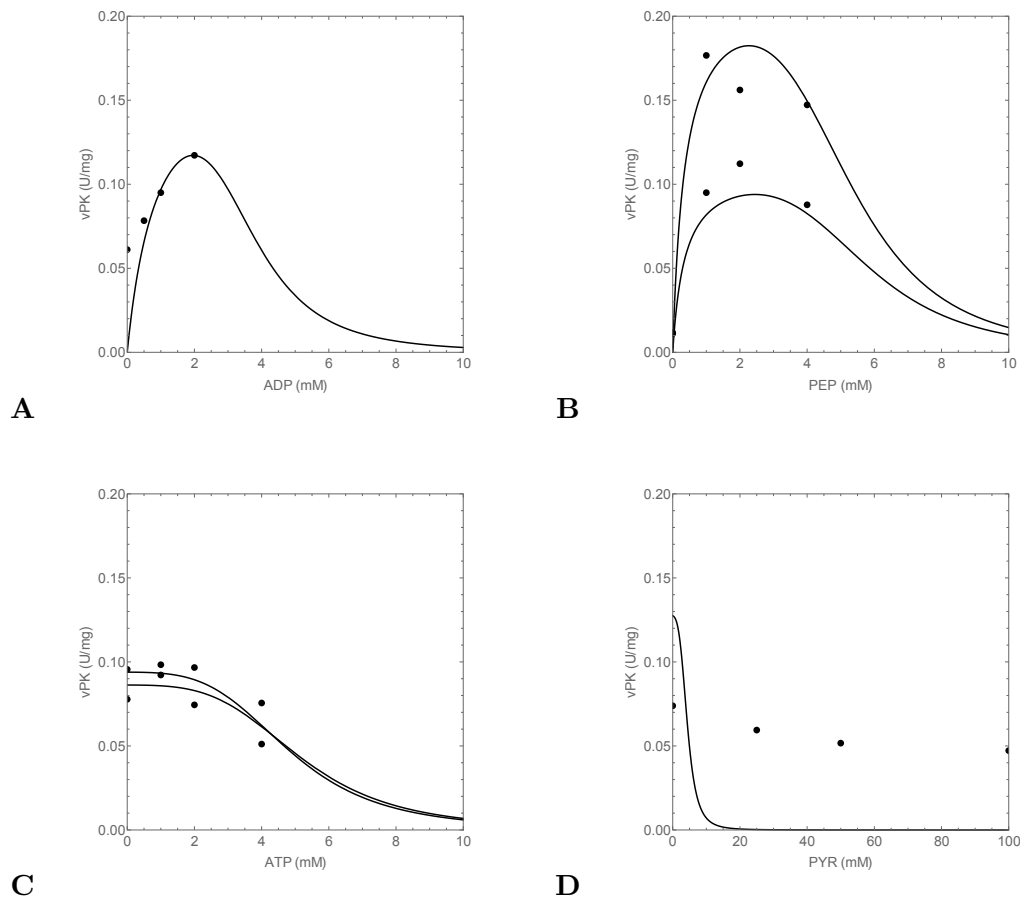


Figure 3.11: Results from the kinetic characterization and subsequent equation fitting of *P. berghei* pyruvate kinase. The velocities of the forward reaction of PK, in terms of the substrates, (A) ADP and (B) PEP, are shown with the inhibition of the products, (C) ATP and (D) Pyr. Equations 3.14 and 3.15 is fitted to the data set to produce the fitted lines that does not describe the data set well (adjusted $R^2 = 0.86$).

that could not be measured was used from the work of Penkler *et al.* (2015). The reasons for the incomplete characterizations will need to be investigated further to complete a full kinetic parameter study. For further refining of parameters, the kinetic assays will need to be repeated to collect more data points and the linking enzymes varied to confirm that they do not hinder the maximal velocities of the reactions by using saturated substrate positive controls. The data obtained was used in the creation of a glycolytic model which will be discussed in chapter 4. All the kinetic parameters obtained are compared to the values obtained from the kinetic study of *P. falciparum* done by Penkler *et al.* (2015). The majority of the kinetic parameters obtained for *P. berghei* differ to the values for *P. falciparum* by a factor between two and four. Differences in the kinetic parameters could be because of the different enzymatic activities for the two species, but could also be due to prolonged storage degradation before the experiments were performed. Two enzymes show noticeable differences to the work of Penkler *et al.* (2015), namely

Table 3.11: Enzyme kinetic parameters for *P. berghei* LDH. The Michaelis constants for the different metabolites and the maximal velocities of the forward and reverse reaction that were fitted using the data in figure 3.12 and equation 3.16 are displayed in the table alongside the values Penkler *et al.* (2015) fitted or used for *P. falciparum*. The asymptotic standard error is given with all the fitted values.

Parameter	Fitted Value	Literature value
V_f ($\mu\text{mol}\cdot\text{min}^{-1}\cdot\text{mg}^{-1}$)	1.35 ± 0.04	2.5 ± 0.1
V_r ($\mu\text{mol}\cdot\text{min}^{-1}\cdot\text{mg}^{-1}$)	0.65 ± 0.94	1.4 ± 0.2
K_{nadh} (mM)	0.040 ± 0.006	0.046 ± 0.003
K_{pyr} (mM)	0.093 ± 0.027	0.13 ± 0.01
K_{lac} (mM)	22 ± 35	3.6 ± 0.3
K_{nad+} (mM)	0.95 ± 1.15	0.23 ± 0.02
K_{eq} (mM)	11959	150-430

ALD and GAPDH, which will be discussed further in the next chapter.

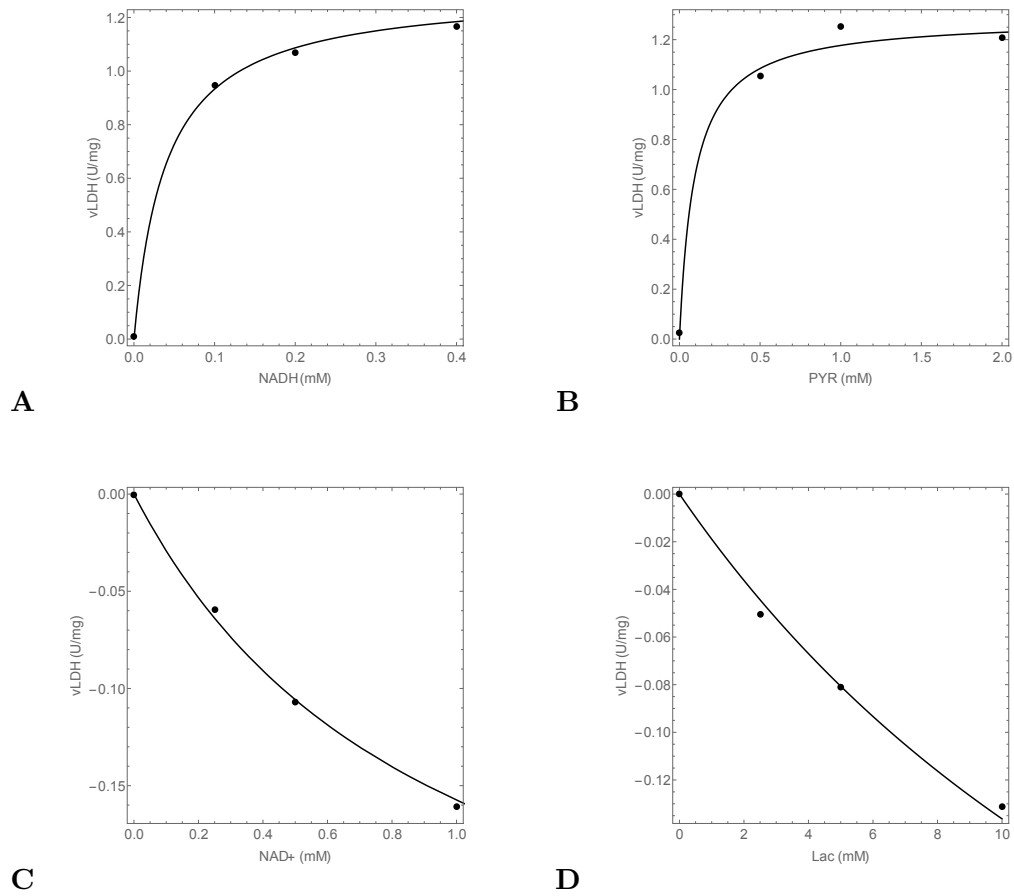


Figure 3.12: Results from the kinetic characterization and subsequent equation fitting of *P. berghei* lactate dehydrogenase. The velocities of the forward reactions of LDH, measured by varying the enzyme substrates, (A) NADH and (B) PYR, concentrations is shown with the velocities of the reverse reaction, measured by varying the enzyme product concentrations, (C) NAD⁺ and (D) Lac. Equation 3.16 is fitted to the data set to produce the fitted lines that describes the data well (adjusted $R^2 = 1.00$).

Table 3.12: A summary of kinetic parameters obtained from the kinetic characterization of the glycolytic enzymes. The different K_m 's (mM), K_{eq} 's and V_{max} 's ($\mu\text{mol}\cdot\text{min}^{-1}\cdot\text{mg}^{-1}$) for both the forward and reverse direction where measured are shown in the table. Data points with an asterix next to the numbers are taken from the work of Penkler *et al.* (2015). The data are used in the creation of the model in chapter 4.

	HK	GPI	PFK	ALD	TPI	GAPDH	PGK	PGM	ENO	PK	LDH
V_f	0.47	1.77	2.1	0.013	-	0.14	-	0.25	0.56	0.36	1.35
V_r	-	0.29	-	-	5.1	-	0.64	-	-	-	0.65
K_{glu}	0.33	-	-	-	-	-	-	-	-	-	-
K_{g6p}	0.064	2.06	-	-	-	-	-	-	-	-	-
K_{f6p}	-	0.19	0.21	-	-	-	-	-	-	-	-
K_{f16bp}	-	-	3.2	0.029	-	-	-	-	-	-	-
K_{dhap}	-	-	-	0.11*	2*	-	-	-	-	-	-
K_{gap}	-	-	-	0.05*	0.5	0.9*	-	-	-	-	-
K_{b13pg}	-	-	-	-	-	0.55	0.013*	-	-	-	-
K_{pg3}	-	-	-	-	-	-	0.06	3.	-	-	-
K_{pg2}	-	-	-	-	-	-	-	0.32*	0.62	-	-
K_{pep}	-	-	-	-	0.016*	-	-	-	1.3*	0.36	-
K_{pyr}	-	-	-	-	-	-	-	-	-	-	0.093
K_{lac}	-	-	-	-	-	-	-	-	-	-	22.
K_{nad}	-	-	-	-	-	0.57*	-	-	-	-	0.95
K_{nadh}	-	-	-	-	-	0.029	-	-	-	-	0.04
K_{adp}	0.51	-	0.09	-	-	-	0.33	-	-	0.92	-
K_{atp}	1.5	-	3.6	-	-	-	1.5	-	-	-	-
$K_{i\text{pep}}$	-	-	-	-	-	-	-	-	-	3.3	-
$K_{i\text{pyr}}$	-	-	-	-	-	-	-	-	-	3.19	-
$K_{i\text{adp}}$	-	-	-	-	-	-	-	-	-	2.9	-
$K_{i\text{atp}}$	-	-	-	-	-	-	-	-	-	3.3	-
K_{eq}	1310*	0.55	0.09	0.09*	0.08*	0.0035*	3200*	0.3*	5.7*	-	11959.

Chapter 4

Model construction

4.1 Introduction

Characterizing the kinetic parameters of the different glycolytic enzymes of *P. berghei* proved feasible in the previous chapter. To further validate the feasibility, the creation of a draft metabolic model capable of adequately describing the flux through the metabolic pathway, would serve as proof that kinetic parameter characterization is possible.



Consider reaction 4.1, identical to the reaction use in chapter 3 (eq 3.1). The change in metabolite, X, could be equated using equation 4.2, which shows that the change in concentration X over time is due to the velocity of the creation of X from v_1 and the consumption of X due to v_2 . The change in metabolite concentration as a function of the different enzymes acting on the metabolite is called an ordinary differential equation (ODE). Combining the ODEs for multiple steps in a system creates a simplistic understanding of the change in concentration of each intermediary metabolite in a system when the kinetic parameters of each step is known (Dreyer, 1993).

$$\frac{dx}{dt} = v_1 - v_2 \quad (4.2)$$

The focus of this chapter is to investigate the feasibility of constructing a glycolytic model of *P. berghei*. The creation of the model required of a set of ODEs from the 11 enzymatic steps of glycolysis, a set of starting metabolite concentrations and the kinetic parameters for all the enzymes catalysing the different reactions. If the created model is capable of adequately predicting the steady state flux and metabolite concentration of the system, the construction of a glycolytic model would prove feasible.

Mathematical analysis, metabolic control analysis, of the enzyme velocities could lead to a more in depth understanding of the flux through the system as a whole and control each enzyme has over the flux (Fell and Sauro, 1990). Equation 4.3 demonstrates the classic view of flux control analysis of the system. By perturbing

the velocity of a reaction, the control the enzyme has over the flux through the system could be calculated. All the control coefficients for each enzyme equates to 1. The enzyme that constitutes the most control over the system could targeted for anti-malarial drug development, should the enzyme be sufficiently different to that of the human orthologue. The rationale for the weakness is that a small decrease in the function of the enzyme could have devastating effects on the flux through the whole system and potentially kill the organism.

$$C_{v_i}^J = \frac{d\text{Ln}J}{d\text{Ln}v_i} \quad (4.3)$$

4.2 Methods

4.2.1 Mathematical modeling

A mathematical model of the glycolytic enzymes measured in chapter 3 was created. For the creation of the model a set of 12 ordinary differential equations (ODEs) was created (eqns 4.4 to 4.15) which describe the changes in metabolite concentrations at a specific time interval. The change in a metabolite concentration are dependent on the velocity of the creation and removal of the metabolite catalysed by the different enzymes associated with the metabolite. The velocities of the different enzymes are described by eqns 4.17 to 4.28 which were discussed in chapter 3. The kinetic parameters for each of the reactions is summarized in table 3.12 and the starting concentration of each metabolite is stated in table 4.1. Computational modelling was done using the NDSolve function of Mathematica version 10.0 and the Time evolution function of JWS Online (found online at jjj.bio.vu.nl).

$$\text{g6p}'(t) = v\text{HK} - v\text{GPI} \quad (4.4)$$

$$\text{f6p}'(t) = v\text{GPI} - v\text{PFK} \quad (4.5)$$

$$\text{f16bp}'(t) = v\text{PFK} - v\text{ALD} \quad (4.6)$$

$$\text{dhap}'(t) = v\text{ALD} - v\text{TPI} \quad (4.7)$$

$$\text{gap}'(t) = v\text{ALD} - v\text{GAPDH} + v\text{TPI} \quad (4.8)$$

$$\text{b13pg}'(t) = v\text{GAPDH} - v\text{PGK} \quad (4.9)$$

$$\text{pg3}'(t) = v\text{PGK} - v\text{PGM} \quad (4.10)$$

$$\text{pg2}'(t) = v\text{PGM} - v\text{ENO} \quad (4.11)$$

$$\text{pep}'(t) = v\text{ENO} - v\text{PK} \quad (4.12)$$

$$\text{pyr}'(t) = v\text{PK} - v\text{LDH} \quad (4.13)$$

$$\text{nad}'(t) = v\text{LDH} - v\text{GAPDH} \quad (4.14)$$

$$\text{nadh}'(t) = v\text{GAPDH} - v\text{LDH} \quad (4.15)$$

4.2.2 Constraints, assumptions and conserved moieties

The model is assumed to be a closed system with no compartmentalization and no export or import of metabolites. Owing to the fact that the transporters have not been characterized, the change in glucose and lactate concentrations could not

be described mathematically. The concentrations of glucose and lactate was kept constant at the model starting concentrations. The kinetics of ATPase were not measured, requiring the use of constant ATP and ADP concentrations. NADH and NAD⁺ concentration is considered to be in conserved moiety defined as the total concentration of the two metabolites would always add up to the same concentration, described in eq 4.16.

$$\text{NAD}_{total} = \text{NAD}^+ + \text{NADH} \quad (4.16)$$

Table 4.1: Starting concentrations (mM) for the different fixed and variable metabolites used for model creation.

Metabolite	Concentration (mM)
G6P	0.028
F6P	0.28
F16BP	0.28
DHAP	0.28
GAP	0.28
B13BP	0.28
PG3	0.28
PG2	0.28
PEP	2.8
Pyr	2.8
NAD ⁺	0.7
NADH	0.3
Glu*	5.0
Lac*	0.1
ADP*	0.5
ATP*	1.5

4.2.3 Model analysis

Steady state concentrations for the variable metabolites and steady state enzyme fluxes were calculated using the FindRoot function of Mathematica version 10.0. The flux control matrix of the model was created and calculated using the Flux control matrix function from JWS Online (found online at jjj.bio.vu.nl).

$$v_{HK} = \frac{\frac{glu_i \cdot HK_{Vf} \cdot atp[t]}{HK_{Katp} \cdot HK_{Kglu}} - \frac{HK_{Vf} \cdot adp[t] \cdot g6p[t]}{HK_{Katp} \cdot HK_{Kceq} \cdot HK_{Kglu}}}{\left(\frac{atp[t]}{HK_{Katp}} + 1\right) \left(\frac{adp[t]}{HK_{Kadp}} + \frac{atp[t]}{HK_{Katp}} + 1\right) \left(\frac{g6p[t]}{HK_{Kg6p}} + \frac{glu_i}{HK_{Kglu}} + 1\right)}$$

(4.17)

$$v_{GPI} = \frac{\frac{GPI_{Vf} \cdot g6p[t]}{GPI_{Kg6p}} - \frac{GPI_{Vf} \cdot f6p[t]}{GPI_{Kf6p}}}{\left(\frac{g6p[t]}{GPI_{Kg6p}} + 1\right) \left(\frac{f6p[t]}{GPI_{Kf6p}} + \frac{g6p[t]}{GPI_{Kg6p}} + 1\right)}$$

(4.18)

$$v_{PFK} = \frac{PFK_{Vf} \cdot atp[t] \cdot f6p[t]}{PFK_{Katp} \cdot PFK_{Kf6p} \cdot \left(\frac{atp[t]}{PFK_{Katp}} + 1\right) \left(\frac{adp[t]}{PFK_{Kadp}} + \frac{atp[t]}{PFK_{Katp}} + 1\right) \left(\frac{f16bp[t]}{PFK_{Kf16bp}} + \frac{f6p[t]}{PFK_{Kf6p}} + 1\right)}$$

(4.19)

$$v_{ALD} = \frac{ALD_{Vf} \cdot f16bp[t] \left(1 - \frac{dhap[t] \cdot gap[t]}{ALD_{Kceq} \cdot f16bp[t]}\right)}{ALD_{Kf16bp} \left(\frac{dhap[t] \cdot gap[t]}{ALD_{Kdhap} \cdot ALD_{Kgap}} + \frac{dhap[t]}{ALD_{Kdhap}} + \frac{f16bp[t]}{ALD_{Kf16bp}} + \frac{gap[t]}{ALD_{Kgap}} + 1\right)}$$

(4.20)

$$v_{TPI} = \frac{\frac{TPI_{Kceq} \cdot TPI_{Vf} \cdot dhap[t]}{TPI_{Kgap}} - \frac{TPI_{Vf} \cdot gap[t]}{TPI_{Kgap}}}{\frac{dhap[t]}{TPI_{Kdhap}} + \frac{gap[t]}{TPI_{Kgap}} + \frac{pep[t]}{TPI_{Kipep}} + 1}$$

(4.21)

$$v_{GAPDH} = \frac{\frac{GAPDH_{Kceq} \cdot GAPDH_{Vf} \cdot gap[t] \cdot nadh[t]}{GAPDH_{Kb13pg} \cdot GAPDH_{Kceq}} - \frac{GAPDH_{Kb13pg} \cdot GAPDH_{Kceq} \cdot nadh[t]}{GAPDH_{Kb13pg} \cdot GAPDH_{Kceq}}}{\left(\frac{b13pg[t]}{GAPDH_{Kb13pg}} + \frac{gap[t]}{GAPDH_{Kgap}} + 1\right) \left(\frac{nadh[t]}{GAPDH_{Kceq}} + \frac{nadh[t]}{GAPDH_{Kceq}} + 1\right)}$$

(4.22)

$$vPGK = \frac{PGK_{K_{eq}} \cdot PGK_{V_r} \cdot \text{adp}[t] \cdot \text{b13pg}[t] - PGK_{V_r} \cdot \text{atp}[t] \cdot \text{pg3}[t]}{PGK_{K_{atp}} \cdot PGK_{K_{pg3}} - PGK_{K_{atp}} \cdot PGK_{K_{pg3}}} \\ \left(\frac{\text{atp}[t]}{PGK_{K_{atp}}} + \frac{\text{pg3}[t]}{PGK_{K_{pg3}}} + 1 \right) \left(\frac{\text{b13pg}[t]}{PGK_{K_{b13pg}}} + \frac{\text{pg3}[t]}{PGK_{K_{pg3}}} + 1 \right) \quad (4.23)$$

$$vPGM = \frac{PGM_{V_r} \cdot \text{pg3}[t] - PGM_{K_{eq}} \cdot PGM_{K_{pg3}}}{PGM_{K_{pg2}} + \frac{\text{pg3}[t]}{PGM_{K_{pg3}}} + 1} \quad (4.24)$$

$$vENO = \frac{ENO_{V_r} \cdot \text{pg2}[t] - ENO_{K_{eq}} \cdot ENO_{K_{pg2}}}{\frac{\text{pg2}[t]}{ENO_{K_{pg2}}} + \frac{\text{pg2}[t]}{ENO_{K_{pg2}}} + 1} \quad (4.25)$$

$$vPK = \frac{PK_{V_r} \cdot \text{adp}[t] \cdot \text{pep}[t]}{PK_{K_{adp}} \cdot PK_{K_{pep}} \left(\frac{\text{adp}[t]}{PK_{K_{adp}}} + \frac{\text{pep}[t]}{PK_{K_{pep}}} + 1 \right) \left(PK_{L0} \left(\left(\frac{\text{adp}[t]}{PK_{K_{iadp}}} + \frac{\text{atp}[t]}{PK_{K_{iatp}}} \right)^n + 1 \right) \left(\left(\frac{\text{pep}[t]}{PK_{K_{ipep}}} + \frac{\text{pyr}[t]}{PK_{K_{ipyr}}} \right)^n + 1 \right) + 1 \right)} \quad (4.26)$$

$$vLDH = \frac{LDH_{V_r} \cdot \text{nadh}[t] \cdot \text{pyr}[t] - \text{lac}_i \cdot LDH_{V_r} \cdot \text{nadh}[t]}{LDH_{K_{nadh}} \cdot LDH_{K_{pyr}} - LDH_{K_{lac}} \cdot LDH_{K_{nadh}}} \\ \left(\frac{\text{lac}_i}{LDH_{K_{lac}}} + \frac{\text{pyr}[t]}{LDH_{K_{pyr}}} + 1 \right) \left(\frac{\text{nadh}[t]}{LDH_{K_{nadh}}} + \frac{\text{nadh}[t]}{LDH_{K_{nadh}}} + 1 \right) \quad (4.27)$$

$$(4.28)$$

4.3 Results and Discussion

A mathematical model of the glycolytic pathway was constructed using the NDSolve function of Mathematica version 10.0. For the construction of the model, a set of ordinary differential equations was used (eqns 4.4 to 4.15) that described the change for each variable metabolite in the glycolytic pathway according to the velocities of each glycolytic enzyme (eqns 4.17 to 4.28) that was bound by the kinetic parameters measured in chapter 3 (table 3.12) and the starting metabolite concentrations (table 4.1).

Figure 4.1 shows the change of each of the variable metabolites concentration per time iteration as a time course of the model presented by JWS. Only after 2500 time iterations did the model reach a stable steady state, thus requiring further analysis. Modelling with Mathematica version 10.0 delivered similar results (figure C.-1) which, because of the size of the graphical representation of the flux, is displayed in appendix C. Steady state concentration for the different metabolites of the draft model is displayed next to the time course, 4.1. As observed from the velocities of the initial model, the concentration for F16BP far exceeds biological concentrations; also reflected by examining the steady state metabolite concentrations (figure 4.1). It appears that the initial model failed, but JWS allowed this researcher to create a metabolic control analysis heat map (figure 4.2) to interpret the control each glycolytic enzyme had on the flux of the model. The darker the bands are on figure 4.2, the greater the control the specific enzyme has on the flux as a whole. Results from the flux control analysis indicated that GAPDH and aldolase had the greatest control (78.3%) over the whole model. As previously discussed in the results from chapter 3, the two enzymes had the greatest difference in V_f 's compared to the work of Penkler *et al.* (2015).

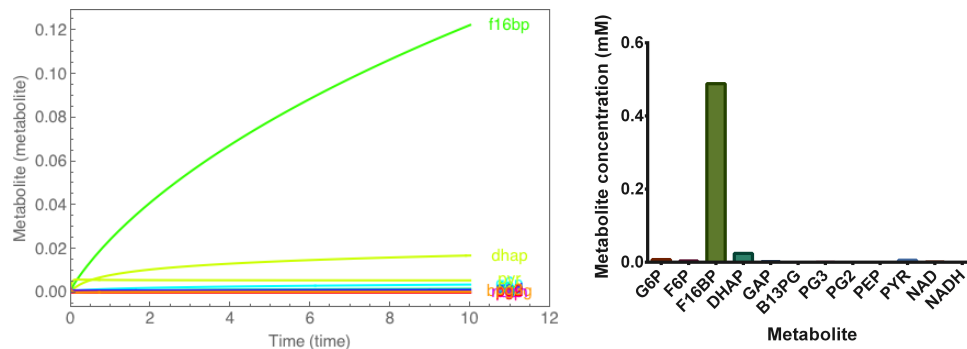


Figure 4.1: Metabolite concentrations for model over time course from JWS Online and steady state concentrations. The different glycolytic intermediate metabolites are shown as a function of time iterations (minutes) and the metabolite steady state concentrations shown on the bar graph on the right. The equations and enzyme kinetic parameters are described in text. The concentration of F16BP does not reach a steady state in 10 time iterations and the concentration increases beyond physiological conditions. The model does not accurately describe the change of intermediate metabolites for the different *P. berghei* glycolytic enzymes

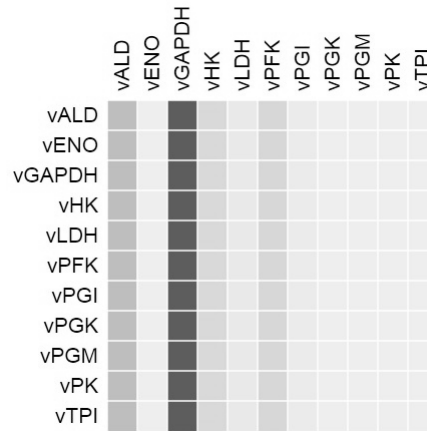


Figure 4.2: A heat map created by JWS online that shows the difference in relative flux control the different enzymes have on the glycolytic model using the concentration control matrix function. The band shade intensity indicates the relative percentage control the enzyme has on the flux of the system. Aldolase and GAPDH seems to have majority control over the flux through the system and would explain the concentrations of the metabolites that fall outside of biological standards in table 4.2

Since this particular project is focussed on the feasibility of creating a full and accurate model, the model was reconstructed with the maximal velocities for aldolase and GAPDH from the work of Penkler *et al.* (2015), rather than the fitted values obtained from the characterization of the different enzymes, using JWS online and Mathematica (figure 4.3). The recreated model reaches steady state in fewer time iterations compared to that of the previous model with steady concentrations that closer reflect that of biological possible conditions (table 4.2 and bar graph on figure 4.3). The flux for each enzyme and steady state concentrations are given for both models in table 4.2 and 4.3. Steady state flux of the new model is 4 times greater than the flux of the original model and the combined control aldolase and GAPDH have over the system flux decreased to 30%. Flux values from Penkler *et al.* (2015) (0.265 and 0.509) are 6 times greater than the flux values obtained for *P. berghei*.

Creation of a working model required a few assumptions that included the complete conversion of glucose to lactate and no influence of auxiliary pathways, for example the pentose or glycerol pathway. Some metabolites, including ATP, ADP, Glu and Lactate, were constrained to specific concentrations, which reflect biological conditions, but the true steady state concentrations of these metabolites is not known. The entire model is placed in one uniform compartment; but this does not hold true for biological life, as certain pathways are compartmentalised, but for the purpose of creating the model, one uniform compartment is sufficient.

4.3.1 Summary

Creation of a working model appears to be feasible and worth further investigation and improvement. The draft model was altered to use the V_f values for Aldolase and GAPDH from the work of Penkler *et al.* (2015) and the model reached adequate steady state within acceptable biological steady state concentrations. A complete

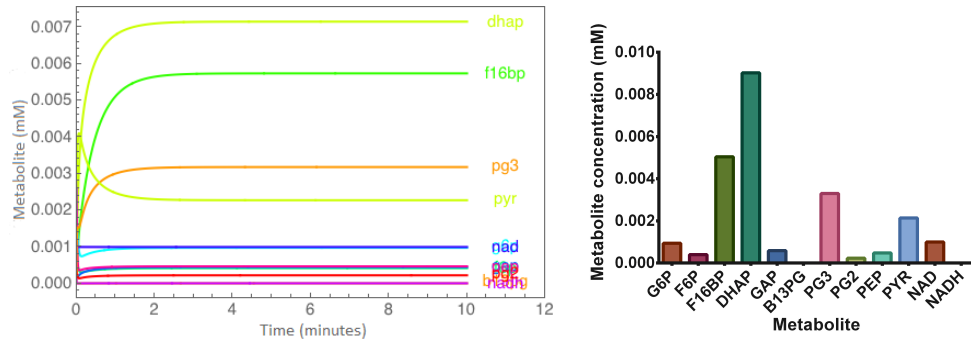


Figure 4.3: Metabolite concentrations for the corrected model over time course from JWS Online and steady state concentrations. The different glycolytic intermediate metabolites are shown as a function of time iterations and the steady state metabolite concentrations on the bar graph on the right. The equations and enzyme kinetic parameters are described in text. The concentrations of the intermediate metabolites, summarized in table 4.2, fall within the physiological range. The model reaches steady state faster than the previous model.

Table 4.2: Model steady state metabolites concentrations. The variable metabolite concentrations of the first and corrected model are displayed below. The concentrations (mM) were calculated using Mathematica's find root function.

Metabolite	Steady state concentration of the glycolytic model (mM)	Steady state concentration of the recreated glycolytic model (mM)
G6P	7.28	0.94
F6P	3.51	0.40
F16BP	488	5.0
DHAP	23.9	9.0
GAP	1.88	0.59
B13PG	4.73×10^{-4}	4.88×10^{-3}
PG3	0.44	0.33
PG2	0.051	0.23
PEP	0.16	0.48
Pyr	5.50	2.14
NAD ⁺	1.00	1.00
NADH	1.08×10^{-3}	5.06×10^{-3}

working model will require a complete characterization of the glycolytic enzymes that could be achieved with multiple repeats of the characterization with different *P. berghei* extracts. Validation of the glycolytic model will also be necessary to prove that the glycolytic model could adequately describe the glucose flux through the parasite; both for the intact parasite and the infected red blood cell. The model will also need to be expanded to include the glucose, lactate, glycerol, pyruvate transporters and the kinetic characterization of the RBCs enzymes, along with appropriate compartmentalization and auxiliary pathways, to create a network-level *P. berghei* model.

Table 4.3: Flux ($\mu\text{mol}\cdot\text{min}^{-1}\cdot\text{mg}^{-1}$) of the different enzymes for both the first and corrected glycolytic model. The fluxes were calculate using Mathematica's NDSolve function.

Enzyme	Steady state flux of the glycolytic model($\mu\text{mol}\cdot\text{min}^{-1}\cdot\text{mg}^{-1}$)	Steady state flux of the corrected glycolytic model($\mu\text{mol}\cdot\text{min}^{-1}\cdot\text{mg}^{-1}$)
HK	0.0087	0.038
GPI	0.0087	0.038
PFK	0.0087	0.038
ALD	0.0087	0.038
TPI	0.0087	0.038
GAPDH	0.017	0.075
PGK	0.017	0.075
PGM	0.017	0.075
ENO	0.017	0.075
PK	0.017	0.075
LDH	0.017	0.075

Chapter 5

General discussion, future work and conclusion

The goal of this project was to evaluate the feasibility of constructing a whole body rat model infected with *P. berghei*. Analysing the feasibility required the acquisition of blood and kinetic parameters, the creating of a preliminary model to assess if the metabolic data could be measured and mathematically described using a molecular and systems biology approach. Four objectives were set: First, we had to inoculate rats with *P. berghei* and be able to obtain blood parameters, including blood glucose, lactate, haematocrit and parasitemia, over the course of the infection. The blood glucose and lactate homeostasis of the rats were then perturbed to assess if it is possible to measure homeostatic potential. Should measuring the blood parameters be possible, the possibility of constructing a whole body model that could describe the changes over the course of the infection would be investigated. The second and third objectives focussed on the prospect of isolating intact parasites and the enzymes contained in the parasite to quantify the kinetic parameter of each enzyme. Lastly, the fourth objective was to construct a working glycolytic model with the kinetic parameters obtained from the kinetic studies

In chapter 2, "Rat blood analysis", we demonstrated that it is possible to inoculate rats with *P. berghei*, ANKA strain, and obtain blood parameters from the rats. Microscopy and enzymatic glucose and lactate determination proved to be reliable and accurate methods to measure these blood parameters. Further improvements in the methodology need to be implemented for more accurate glucose and lactate concentration measurement as large variability was found for the concentrations. Reasons for the variability could be because of the panicked state of the rats resulting in agitation and spikes in the lactate concentrations. Methods to improve the accuracy of the blood parameter data collection includes anaesthesia of the rats during all blood collection experiments and environmental changes to keep the animals calm. Rat subjects could also be calmed inducing tolerance to handling a month prior to the experiments. The growth of the parasites and decrease in haematocrit displayed predictable patterns, allowing us to quantify the relationship between haematocrit and parasitemia. Although the measuring of the blood glucose and lactate concentrations proved possible, the results obtained from the pulse experiments and the lactate concentration determination did not present

with a distinct pattern and therefore, measuring of the blood changes needs to be repeated and the mechanism of homeostasis investigated in more detail.

Isolation of the parasites, isolation of the glycolytic enzymes from sufficient biomass and kinetic parameter quantification proved practicable. In chapter 3, all the glycolytic enzymes of *P. berghei* were characterized in terms of their K_m 's, V_{max} 's and K_{eq} 's. The results of the enzymatic characterizations were compared to the enzymatic parameters *P. falciparum* characterized by Penkler *et al.* (2015), which showed some similarities. The maximal velocities of GAPDH and ALD are significantly lower than that of Penkler *et al.* (2015), indicating the need for improvement of the experimental design. Due to limitations in the amount of biological samples available, the limited data points of the kinetic characterization forestall the publication the kinetic parameters, necessitating refinements and repeating of the work.

With the kinetic parameters obtained in chapter 3, a glycolytic model was created to assess the feasibility of constructing a model that could adequately describe the flux through *P. berghei* glycolysis in chapter 4. The feasibility of constructing the model depends on the ability of the model to predict steady state metabolite concentrations that reflect the intercellular metabolite concentrations of the parasite. The first attempt at constructing a model using the experimentally obtained kinetic parameters did not satisfactory predict the steady state concentrations and flux. Using MCA, the enzymes with the most control over the system, ALD and GAPDH, were identified. Since the project is focussed on the feasibility of constructing a model and not about the construction of a flawless model, the kinetic parameters of ALD and GAPDH from the work of Penkler *et al.* (2015) were used for the construction of a revised model. Near physiological steady state concentrations were predicted by the revised model, proving that the construction of a model is feasible. Perfecting the kinetic parameter quantification will lead to an increased precision of the model.

Various strategies could be implemented to improve our knowledge of the preliminary model and the metabolism of a rat infected with *P. berghei*: Respiratory changes of rats infected with malaria could be modelled using a metabolic chamber for the rats that calculates the oxygen consumption by measuring the the carbon dioxide formation; the internal lactate uptake of the body could be better understood by attaching lactate biosensors to the liver of the rats; *in vitro* cultivation of the parasite would allow for validations of the model by measuring the flux and comparing it to the model predicted values; expansion of the model by including the metabolism, transporters and compartmentalization of the RBC and the auxiliary pathways of the parasite and the flux obtained from the glycolytic model could be validated by measuring the glucose consumption and lactate production of intact parasites.

In conclusion, the aims and objectives of the project have been met; a summation follows: The rats were infected with *P. berghei* and the blood parameters were measured. Relationships between the different parameters and parasitemia were also investigated. Measuring the homeostatic potential of the rat's metabolism proved to be possible for the glucose pulse experiments, but not for the lactate pulse experiment. Since no differences could be measured between the infected and non-infected glucose pulse experiments, quantification of the effect the

infection has on the homeostatic potential could not be performed. However limited the quantification of the relationships and homeostatic potential, the determination of the different parameters gives evidence enough to assume that the body model is feasible. Furthermore, the characterization of the glycolytic enzymes displayed similar results to that of the work of Penkler *et al.* (2015), giving rise to the assumption that creating a glycolytic model is practicable. A glycolytic model was then successfully constructed, capable of predicted steady-state metabolic concentrations that fall within biological ranges. Although the accuracy of the model could only be validated by comparing the flux of the model to the glucose flux of intact parasites, the successful construction of the model proves that glycolytic model construction is possible, but incomplete, for no validations were performed. From the above mentioned, the project demonstrated that, with the combination of molecular biology and systems biology, the creation of a whole body model that could describe hypoglycemia and lactic acidosis in rats infected with *P. berghei* is feasible, warranting further investigation. Once the whole metabolism of the parasite is characterized, the progression from single parasite modelling to the creation of a whole body would need to include the effect of parasitemia and the homeostatic capabilities of the rats to a functional model. Many challenges exist when working with *P. berghei*, including extreme difficulties with *in vitro* culturing of the parasite, which could be circumvented if another organism, for example *P. knowlesi*, is used. It should be noted that, although the feasibility of completing such a model is clear, it is not known whether or not the data obtained is accurate as limited repeats of some experiments were performed.

With the creation of a whole body model, a weakness could be identified in the malarial parasite using metabolic control analysis. Once a weakness is discovered, effects of inhibition of the enzyme could be predicted with the model. Use of the model could be extended to serve as a powerful diagnostic tool, as extent of the infection could be calculated if one or more of the blood parameters are known. The promise of high throughput drug development derived from the understanding of the host-parasite interaction on a metabolic level gives reason for the pursuit of creating of a full model for malarial infections and other infectious diseases.

Appendix A

Buffers and Media Composition

Table A.1: Enzyme Assay Buffer (EAB). The components, final concentrations and companies from which the compound were purchased. pH adjusted to final pH of 7.17

Final Concentration	Compound	Company
20 mM	HEPES	Sigma-Aldrich
20 mM	Magnesium Chloride Hexahydrate	Merck
10 mM	Potassium Chloride	Merck
20 mM	Sodium Chloride	Merck

Table A.2: Culture Media (CM). The components, final concentrations and companies from which the compound were purchased. pH adjusted to final pH of 7.25

Final Concentration	Compound	Company
10.4 g/L	RPMI-1640 medium	Simga-aldrich
4 g/L	Glucose	Merck
5 g/L	Albumax II	Thermo Fisher Scientific
2.1 g/L	Sodium Bicarbonate	Simga-aldrich
0.4 g/L	Hypoxanthine	Simga-aldrich
0.05 g/L	Gentamycin Sulphate Salt	Simga-aldrich

Table A.3: Glu-Lac-Determination Buffer (GLDB). The components, final concentrations and companies from which the compound were purchased. pH adjusted to final pH of 7.6

Final Concentration	Compound	Company
150 mM	HEPES	Sigma-aldrich
15 mM	Magnesium Sulphate Heptahydrate	Merck
3.75 %v/v	Hydrazine monohydrate*	Sigma-aldrich

*Hydrazine monohydrate is only added to the Lactate determination buffer and not the Glucose determination buffer

Table A.4: Citrate-phosphate-dextrose-adenine (CPDA) adjusted from Kurup *et al.* (2004). The components, final concentrations and companies from which the compound were purchased. pH adjusted to final pH of 7.6

Final Concentration	Compound	Company
15.2 mM	Citric acid	Merck
87.6 mM	Sodium citrate anhydrous	Saarchem
1.98 mM	Adenine	Calbiochem
1.8 mM	L-ascorbic acid	Sigma-aldrich
4.4 mM	Nicotinic acid	Sigma-aldrich
15.8 mM	Sodium dihydrogen phosphate	Merck
173 mM	Dextrose	Merck

Appendix B

Full Rat Blood Analysis Data

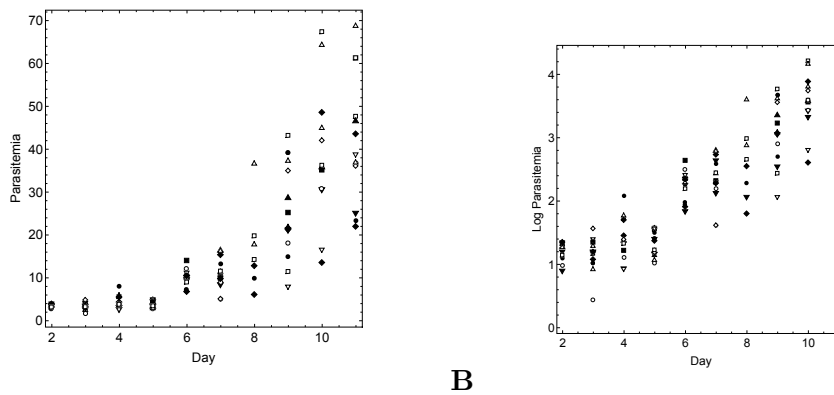


Figure B.1: Full parasitemia measurements. (A) Average parasitemia per day. (B) Log of average parasitemia per day

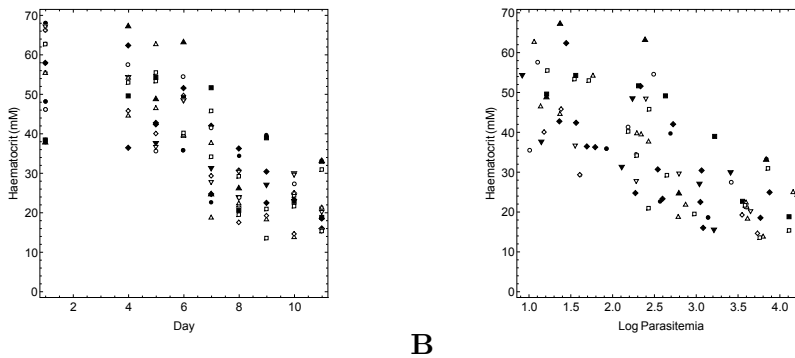


Figure B.2: Full haematocrit measurements. (A) Average haematocrit per day. (B) Haematocrit per log average parasitemia

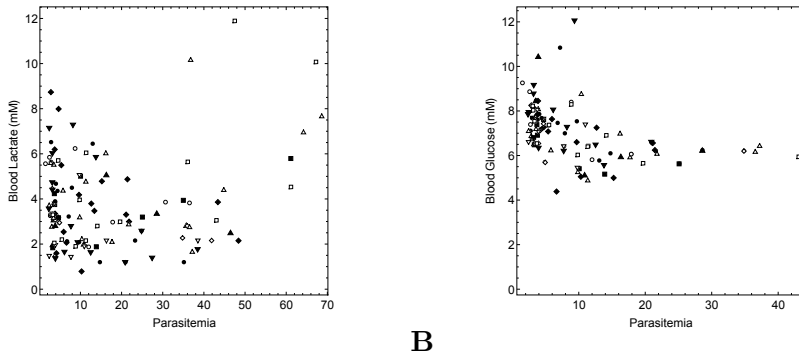


Figure B.3: Full blood glucose and lactate per parasitemia. (A) Blood lactate (mM) per parasitemia. (B) Blood Glucose (mM) per parasitemia.

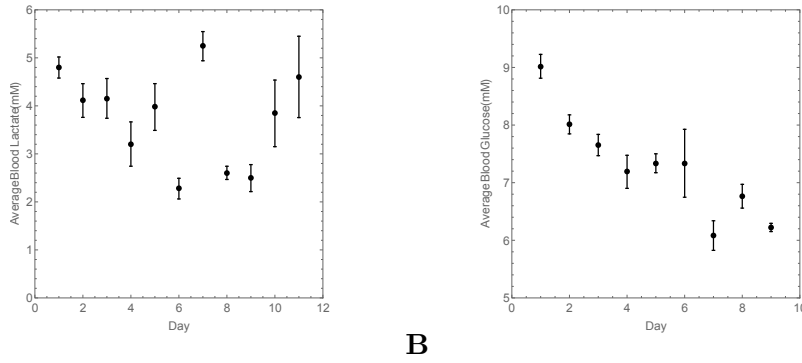
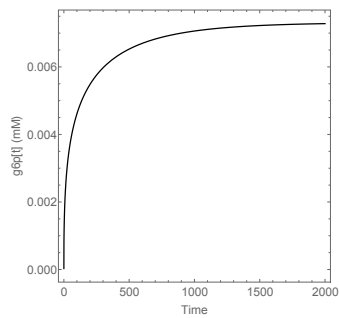


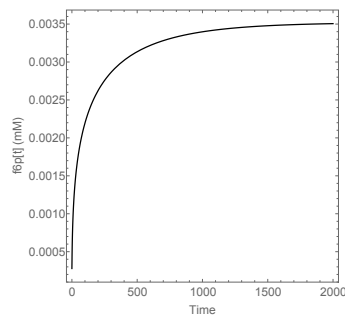
Figure B.4: Full average blood glucose and lactate per day. (A) Average blood Lactate (mM) per day. (B) Average blood Glucose (mM) per day.

Appendix C

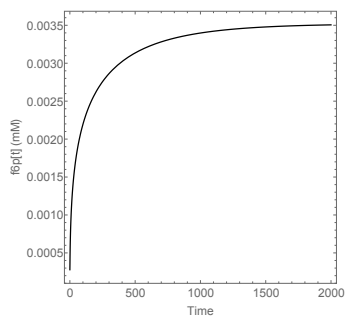
Full model fluxes



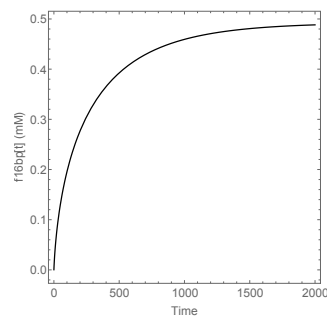
(a) G6P



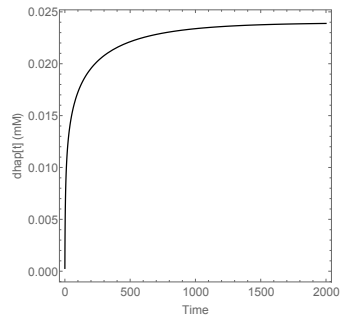
(b) F6P



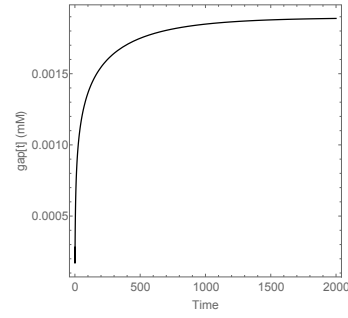
(c) F16BP



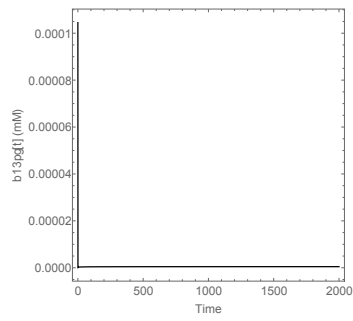
(d) DHAP



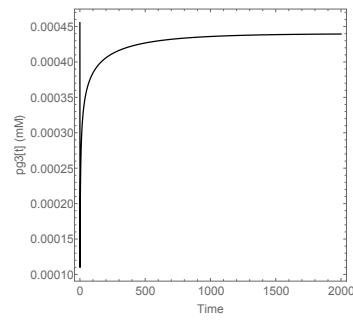
(e) GAP



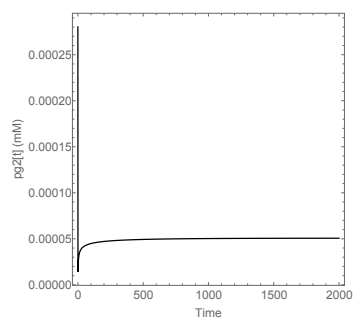
(f) B13PG



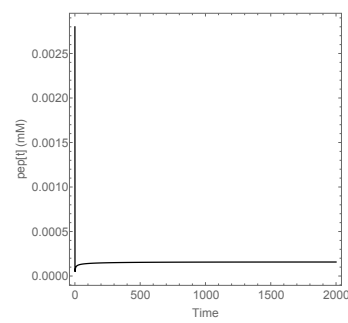
(g) PG3



(h) PG2



(i) PEP



(j) Pyr

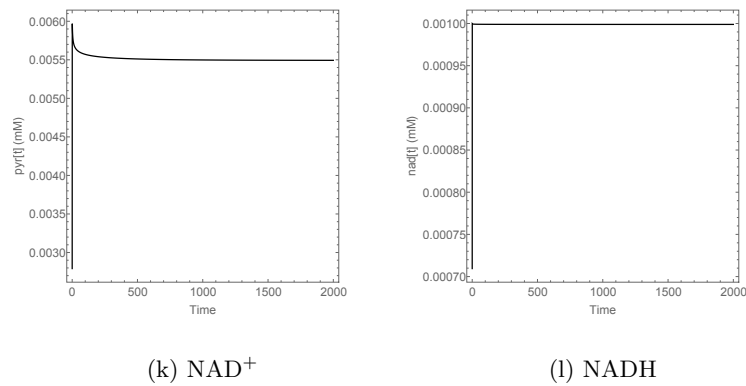


Figure C.-1: Metabolite concentrations of the model over time from Mathematica 10.0. Different substrate concentrations over time as simulated by a computer for the different kinetic parameters and enzyme characteristics. From (A) to (L) the substrates at specific time point include G6P, F6P, F16BP, DHAP, GAP, B13PG, PG3, PG2, PEP, PYR, NAD^+ , NADH respectively. The equations and parameters used for the creation of the model are described in text. The time course extends past 2000 time iterations (minutes) to reach steady state

List of References

- Amino, R., Thiberge, S., Martin, B., Celli, S., Shorte, S., Frischknecht, F. and Ménard, R. (2006). Quantitative imaging of *Plasmodium* transmission from mosquito to mammal. *Nature Medicine*, vol. 12, no. 2, pp. 220–224.
- Archer, G.L. (1998). Staphylococcus aureus: a well-armed pathogen. *Clinical Infectious Diseases*, vol. 26, no. 5, pp. 1179–1181.
- Atamna, H., Pascarmona, G. and Ginsburg, H. (1994). Hexose-monophosphate shunt activity in intact *Plasmodium falciparum*-infected erythrocytes and in free parasites. *Molecular and Biochemical Parasitology*, vol. 67, no. 1, pp. 79–89.
- Atkins, G. and Nimmo, I. (1975). A comparison of seven methods for fitting the michaelis-menten equation. *Biochemical Journal*, vol. 149, no. 3, pp. 775–777.
- Ayi, K., Min-Oo, G., Serghides, L., Crockett, M., Kirby-Allen, M., Quirt, I., Gros, P. and Kain, K.C. (2008). Pyruvate kinase deficiency and malaria. *New England Journal of Medicine*, vol. 358, no. 17, pp. 1805–1810.
- Bannister, L., Butcher, G., Dennis, E. and Mitchell, G. (1975). Structure and invasive behaviour of *Plasmodium knowlesi* merozoites in vitro. *Parasitology*, vol. 71, no. 03, pp. 483–491.
- Baumann, E., Stoya, G., Völkner, A., Richter, W., Lemke, C. and Linss, W. (2000). Hemolysis of human erythrocytes with saponin affects the membrane structure. *Acta Histochemica*, vol. 102, no. 1, pp. 21–35.
- Becker, K., Tilley, L., Vennerstrom, J.L., Roberts, D., Rogerson, S. and Ginsburg, H. (2004). Oxidative stress in malaria parasite-infected erythrocytes: host–parasite interactions. *International Journal for Parasitology*, vol. 34, no. 2, pp. 163–189.
- Bodor, N. and Buchwald, P. (2000). Soft drug design: general principles and recent applications. *Medicinal Research Reviews*, vol. 20, no. 1, pp. 58–101.
- Bowman, I., Grant, P. and Kermack, W. (1960). The metabolism of *Plasmodium berghei*, the malaria parasite of rodents. i. the preparation of the erythrocytic form of *P. berghei* separated from the host cell. *Experimental Parasitology*, vol. 9, no. 2, pp. 131–136.
- Bradford, M.M. (1976). A rapid and sensitive method for the quantitation of microgram quantities of protein utilizing the principle of protein-dye binding. *Analytical Biochemistry*, vol. 72, no. 1, pp. 248–254.

- Buckwitz, D., Jacobasch, G. and Gerth, C. (1990a). Phosphofructokinase from *Plasmodium berghei*: a kinetic model of allosteric regulation. *Molecular and Biochemical Parasitology*, vol. 40, no. 2, pp. 225–232.
- Buckwitz, D., Jacobasch, G. and Gerth, C. (1990b). Phosphofructokinase from *Plasmodium berghei*. Influence of Mg²⁺, ATP and Mg²⁺ (+)-complexed ATP. *Biochem. J.*, vol. 267, pp. 353–357.
- Buckwitz, D., Jacobasch, G., Gerth, C., Holzhütter, H.-G. and Thamm, R. (1988). A kinetic model of phosphofructokinase from *Plasmodium berhei*. Influence of ATP and fructose-6-phosphate. *Molecular and Biochemical Parasitology*, vol. 27, no. 2, pp. 225–232.
- Bzik, D.J., Fox, B.A. and Gonyer, K. (1993). Expression of *Plasmodium falciparum* lactate dehydrogenase in *Escherichia coli*. *Molecular and Biochemical Parasitology*, vol. 59, no. 1, pp. 155–166.
- Campillos, M., Kuhn, M., Gavin, A.-C., Jensen, L.J. and Bork, P. (2008). Drug target identification using side-effect similarity. *Science*, vol. 321, no. 5886, pp. 263–266.
- Carson, P. (1984). 8-aminoquinolines. In: *Antimalarial Drug II*, pp. 83–121. Springer.
- Carter, R. (1970). Enzyme variation in *Plasmodium berghei*. *Transactions of the Royal Society of Tropical Medicine and Hygiene*, vol. 64, no. 3, pp. 401–406.
- Chan, M. and Sim, T.-S. (2004). Functional analysis, overexpression, and kinetic characterization of pyruvate kinase from *Plasmodium falciparum*. *Biochemical and Biophysical Research Communications*, vol. 326, no. 1, pp. 188–196.
- Chulay, J.D., Haynes, J.D. and Diggs, C.L. (1983). *Plasmodium falciparum*: assessment of in vitro growth by [3 h] hypoxanthine incorporation. *Experimental Parasitology*, vol. 55, no. 1, pp. 138–146.
- Coatney, G.R. *et al.* (1963). Pitfalls in a discovery: the chronicle of chloroquine. *American Journal of Tropical Medicine and Hygiene*, vol. 12, no. 2, pp. 121–8.
- Craig, A.G., Grau, G.E., Janse, C., Kazura, J.W., Milner, D., Barnwell, J.W., Turner, G., Langhorne, J. *et al.* (2012). The role of animal models for research on severe malaria. *PLoS Pathog*, vol. 8, no. 2, p. e1002401.
- Cromer, D., Evans, K.J., Schofield, L. and Davenport, M.P. (2006). Preferential invasion of reticulocytes during late-stage *Plasmodium berghei* infection accounts for reduced circulating reticulocyte levels. *International Journal for Parasitology*, vol. 36, no. 13, pp. 1389–1397.
- Daubenberger, C.A., Pörtl-Frank, F., Jiang, G., Lipp, J., Certa, U. and Pluschke, G. (2000). Identification and recombinant expression of glyceraldehyde-3-phosphate dehydrogenase of *Plasmodium falciparum*. *Gene*, vol. 246, no. 1, pp. 255–264.

- Dimopoulos, G., Seeley, D., Wolf, A. and Kafatos, F.C. (1998). Malaria infection of the mosquito *Anopheles gambiae* activates immune-responsive genes during critical transition stages of the parasite life cycle. *The EMBO Journal*, vol. 17, no. 21, pp. 6115–6123.
- Dreyer, T.P. (1993). *Modelling with ordinary differential equations*. CRC Press.
- Emmerling, M., Dauner, M., Ponti, A., Fiaux, J., Hochuli, M., Szyperski, T., Wüthrich, K., Bailey, J. and Sauer, U. (2002). Metabolic flux responses to pyruvate kinase knockout in *Escherichia coli*. *Journal of Biochemical Toxicology*, vol. 184, no. 1, pp. 152–164.
- Enright, M.C., Robinson, D.A., Randle, G., Feil, E.J., Grundmann, H. and Spratt, B.G. (2002). The evolutionary history of methicillin-resistant *Staphylococcus aureus* (MRSA). *Proceedings of the National Academy of Sciences*, vol. 99, no. 11, pp. 7687–7692.
- Fell, D.A. and Sauro, H.M. (1990). Metabolic control analysis. *European Journal of Biochemistry*, vol. 192, no. 1, pp. 183–187.
- Fry, M. and Beesley, J. (1991). Mitochondria of mammalian *Plasmodium* spp. *Parasitology*, vol. 102, no. 01, pp. 17–26.
- Gomez-Arreaza, A., Acosta, H., Quinones, W., Concepción, J.L., Michels, P.A. and Avilán, L. (2014). Extracellular functions of glycolytic enzymes of parasites: Unpredicted use of ancient proteins. *Molecular and Biochemical Parasitology*, vol. 193, no. 2, pp. 75–81.
- Goudar, C.T., Sonnad, J.R. and Duggleby, R.G. (1999). Parameter estimation using a direct solution of the integrated michaelis-menten equation. *Biochimica et Biophysica Acta (BBA)-Protein Structure and Molecular Enzymology*, vol. 1429, no. 2, pp. 377–383.
- Grall, M., Srivastava, I.K., Schmidt, M., Garcia, A.-M., Mauël, J. and Perrin, L.H. (1992). *Plasmodium falciparum*: identification and purification of the phosphoglycerate kinase of the malaria parasite. *Experimental Parasitology*, vol. 75, no. 1, pp. 10–18.
- Haque, A., Best, S.E., Amante, F.H., Ammerdorffer, A., de Labastida, F., Pereira, T., Ramm, G.A. and Engwerda, C.R. (2011). High parasite burdens cause liver damage in mice following *Plasmodium berghei* ANKA infection independently of CD8+ T cell-mediated immune pathology. *Infection and Immunity*, vol. 79, no. 5, pp. 1882–1888.
- Hayward, R.E. (2000). *Plasmodium falciparum* phosphoenolpyruvate carboxykinase is developmentally regulated in gametocytes. *Molecular and Biochemical Parasitology*, vol. 107, no. 2, pp. 227–240.
- Henderson, S.A., Dallman, P.R. and Brooks, G.A. (1986). Glucose turnover and oxidation are increased in the iron-deficient anemic rat. *American Journal of Physiology-Endocrinology and Metabolism*, vol. 250, no. 4, pp. E414–E421.

- Hicks, K.E., Read, M., Holloway, S.P., Sims, P.F. and Hyde, J.E. (1991). Glycolytic pathway of the human malaria parasite *Plasmodium falciparum*: primary sequence analysis of the gene encoding 3-phosphoglycerate kinase and chromosomal mapping studies. *Gene*, vol. 100, pp. 123–129.
- Hills, T., Srivastava, A., Ayi, K., Wernimont, A.K., Kain, K., Waters, A.P., Hui, R. and Pizarro, J.C. (2011). Characterization of a new phosphatase from *Plasmodium*. *Molecular and Biochemical Parasitology*, vol. 179, no. 2, pp. 69–79.
- Holloway, P., Knox, K., Bajaj, N., Chapman, D., White, N., O'Brien, R., Stacpoole, P. and Krishna, S. (1995). *Plasmodium berghei* infection: dichloroacetate improves survival in rats with lactic acidosis. *Experimental Parasitology*, vol. 80, no. 4, pp. 624–632.
- Holloway, P.A., Krishna, S. and White, N.J. (1991). *Plasmodium berghei*: lactic acidosis and hypoglycaemia in a rodent model of severe malaria; effects of glucose, quinine, and dichloroacetate. *Experimental Parasitology*, vol. 72, no. 2, pp. 123–133.
- Hsu, W., Lu, Z. and Hembrough, F. (1985). Effect of xylazine on heart rate and arterial blood pressure in conscious dogs, as influenced by atropine, 4-aminopyridine, doxapram, and yohimbine. *Journal of the American Veterinary Medical Association*, vol. 186, no. 2, pp. 153–156.
- Jacobasch, G., Buckwitz, D., Gerth, C. and Thamm, R. (1989). Regulation of the energy metabolism of *Plasmodium berghei*. *Biomedica Biochimica Acta*, vol. 49, no. 2-3, pp. S289–94.
- Janse, C. and Waters, A. (1995). *Plasmodium berghei*: the application of cultivation and purification techniques to molecular studies of malaria parasites. *Parasitology Today*, vol. 11, no. 4, pp. 138–143.
- Jensen, M.D., Conley, M. and Helstowski, L.D. (1983). Culture of *Plasmodium falciparum*: the role of pH, glucose, and lactate. *The Journal of Parasitology*, pp. 1060–1067.
- Johnston, J.C., Shahidi, N.C., Sadatsafavi, M., Fitzgerald, J.M. *et al.* (2009). Treatment outcomes of multidrug-resistant *Tuberculosis*: a systematic review and meta-analysis. *PloS one*, vol. 4, no. 9, p. e6914.
- Kamiyama, T., Tatsumi, M., Matsubara, J., Yamamoto, K., Rubio, Z., Cortes, G. and Fujii, H. (1987). Manifestation of cerebral malaria-like symptoms in the WM/Ms rat infected with *Plasmodium berghei* strain NK65. *The Journal of Parasitology*, pp. 1138–1145.
- Killick-Kendrick, R. (1974). Parasitic protozoa of the blood of rodents: a revision of *Plasmodium berghei*. *Parasitology*, vol. 69, no. 02, pp. 225–237.
- Kim, H., Certa, U., Döbeli, H., Jakob, P. and Hol, W.G. (1998). Crystal structure of fructose-1, 6-bisphosphate aldolase from the human malaria parasite *Plasmodium falciparum*. *Biochemistry*, vol. 37, no. 13, pp. 4388–4396.

- Kruckeberg, W.C., Sander, B.J. and Sullivan, D.C. (1981). *Plasmodium berghei*: glycolytic enzymes of the infected mouse erythrocyte. *Experimental Parasitology*, vol. 51, no. 3, pp. 438–443.
- Kumar, S. and Banyal, H. (1996). Purification and characterisation of the hexokinase of *Plasmodium berghei*, a murine malaria parasite. *Acta Veterinaria Hungarica*, vol. 45, no. 2, pp. 119–126.
- Kumar, S. and Banyal, H. (1997). Partial purification and characterization of a murine malaria parasite, *Plasmodium berghei* specific aldolase. *Journal of Veterinary Medicine, Series B*, vol. 44, no. 1-10, pp. 495–499.
- Kurup, P., Arun, P., Gayathri, N., Dhanya, C. and Indu, A. (2004). Modified formulation of CPDA for storage of whole blood, and of SAGM for storage of red blood cells, to maintain the concentration of 2, 3-diphosphoglycerate. *Vox Sanguinis*, vol. 86, no. 3, pp. 200–200.
- Makler, M., Ries, J., Williams, J., Bancroft, J., Piper, R., Gibbins, B. and Hinrichs, D. (1993). Parasite lactate dehydrogenase as an assay for *Plasmodium falciparum* drug sensitivity. *The American Journal of Tropical Medicine and Hygiene*, vol. 48, no. 6, pp. 739–741.
- Makler, M.T. and Hinrichs, D.J. (1993). Measurement of the lactate dehydrogenase activity of *Plasmodium falciparum* as an assessment of parasitemia. *The American Journal of Tropical Medicine and Hygiene*, vol. 48, no. 2, pp. 205–210.
- Manguin, S., Bangs, M., Pothikasikorn, J. and Chareonviriyaphap, T. (2010). Review on global co-transmission of human *Plasmodium* species and *Wuchereria bancrofti* by anopheline mosquitoes. *Infection, Genetics and Evolution*, vol. 10, no. 2, pp. 159–177.
- McAlister, R.O. (1977). Time-dependent loss of invasive ability of *Plasmodium berghei* merozoites *in vitro*. *The Journal of Parasitology*, pp. 455–463.
- McDaniel, H.G. and Siu, P.M. (1972). Purification and characterization of phosphoenolpyruvate carboxylase from *Plasmodium berghei*. *Journal of Bacteriology*, vol. 109, no. 1, pp. 385–390.
- Meier, B., Döbeli, H. and Certa, U. (1992). Stage-specific expression of aldolase isoenzymes in the rodent malaria parasite *Plasmodium berghei*. *Molecular and Biochemical Parasitology*, vol. 52, no. 1, pp. 15–27.
- Mellors, A. (1976). The Haldane relationship enzymes & equilibrium. *Biochemical Education*, vol. 4, no. 4, pp. 71–71.
- Miller, L.H. and Su, X. (2011). Artemisinin: discovery from the Chinese herbal garden. *Cell*, vol. 146, no. 6, pp. 855–858.
- Olafsson, P., Matile, H. and Certa, U. (1992). Molecular analysis of *Plasmodium falciparum* hexokinase. *Molecular and Biochemical Parasitology*, vol. 56, no. 1, pp. 89–101.

- Olszewski, K.L. and Llinás, M. (2011). Central carbon metabolism of *Plasmodium* parasites. *Molecular and Biochemical Parasitology*, vol. 175, no. 2, pp. 95–103.
- Pal, B., Pybus, B., Muccio, D.D. and Chattopadhyay, D. (2004). Biochemical characterization and crystallization of recombinant 3-phosphoglycerate kinase of *Plasmodium falciparum*. *Biochimica et Biophysica Acta (BBA)-Proteins and Proteomics*, vol. 1699, no. 1, pp. 277–280.
- Pal-Bhowmick, I., Mehta, M., Coppens, I., Sharma, S. and Jarori, G.K. (2007a). Protective properties and surface localization of *Plasmodium falciparum* enolase. *Infection and Immunity*, vol. 75, no. 11, pp. 5500–5508.
- Pal-Bhowmick, I., Sadagopan, K., Vora, H.K., Sehgal, A., Sharma, S. and Jarori, G.K. (2004). Cloning, over-expression, purification and characterization of *Plasmodium falciparum* enolase. *European Journal of Biochemistry*, vol. 271, no. 23-24, pp. 4845–4854.
- Pal-Bhowmick, I., Vora, H.K. and Jarori, G.K. (2007b). Sub-cellular localization and post-translational modifications of the *Plasmodium yoelii* enolase suggest moonlighting functions. *Malaria Journal*, vol. 6, no. 1, p. 45.
- Parasuraman, S., Raveendran, R., Kesavan, R. *et al.* (2010). Blood sample collection in small laboratory animals. *Journal of Pharmacology and Pharmacotherapeutics*, vol. 1, no. 2, p. 87.
- Parker, R.S., Doyle III, F.J., Peppas, N. *et al.* (1999). A model-based algorithm for blood glucose control in type i diabetic patients. *Biomedical Engineering, IEEE Transactions on*, vol. 46, no. 2, pp. 148–157.
- Parr, C. (1956). Inhibition of phosphoglucose isomerase. *Nature*.
- Parthasarathy, S., Ravindra, G., Balaram, H., Balaram, P. and Murthy, M. (2002). Structure of the *Plasmodium falciparum* triosephosphate isomerase-phosphoglycolate complex in two crystal forms: characterization of catalytic loop open and closed conformations in the ligand-bound state. *Biochemistry*, vol. 41, no. 44, pp. 13178–13188.
- Pedroni, H.C., Bettoni, C.C., Spalding, S.M. and Dalla Costa, T. (2006). *Plasmodium berghei*: Development of an irreversible experimental malaria model in Wistar rats. *Experimental Parasitology*, vol. 113, no. 3, pp. 193–196.
- Pei, Y., Tarun, A.S., Vaughan, A.M., Herman, R.W., Soliman, J., Erickson-Wayman, A. and Kappe, S.H. (2010). *Plasmodium pyruvate* dehydrogenase activity is only essential for the parasite's progression from liver infection to blood infection. *Molecular Microbiology*, vol. 75, no. 4, pp. 957–971.
- Penkler, G., du Toit, F., Adams, W., Rautenbach, M., Palm, D.C., van Niekerk, D.D. and Snoep, J.L. (2015). Construction and validation of a detailed kinetic model of glycolysis in *Plasmodium falciparum*. *FEBS Journal*, vol. 282, no. 8, pp. 1481–1511.

- Penkler, G.P. (2009 December). *Construction and validation of a detailed kinetic model of glycolysis in asexual Plasmodium falciparum: A feasibility study*. Master's thesis, University of Stellenbosch, Available at: <https://scholar.sun.ac.za/handle/10019.1/2298>.
- Peters, W. *et al.* (1970). Chemotherapy and drug resistance in malaria. *Chemotherapy and Drug Resistance in Malaria*.
- Roth Jr, E. (1989). *Plasmodium falciparum* carbohydrate metabolism: a connection between host cell and parasite. *Blood Cells*, vol. 16, no. 2-3, pp. 453–60.
- Roth Jr, E.F., Ruprecht, R.M., Schulman, S., Vanderberg, J. and Olson, J.A. (1986). Ribose metabolism and nucleic acid synthesis in normal and glucose-6-phosphate dehydrogenase-deficient human erythrocytes infected with *Plasmodium falciparum*. *Journal of Clinical Investigation*, vol. 77, no. 4, p. 1129.
- Saliba, K.J. and Kirk, K. (1999). pH regulation in the intracellular malaria parasite, *Plasmodium falciparum* H⁺ extrusion via a V-type H⁺-ATPase. *Journal of Biological Chemistry*, vol. 274, no. 47, pp. 33213–33219.
- Sherman, I.W. (1979). Biochemistry of *Plasmodium* (malarial parasites). *Microbiological Reviews*, vol. 43, no. 4, p. 453.
- Snoep, J.L., Green, K., Eicher, J., Palm, D.C., Penkler, G., du Toit, F., Walters, N., Burger, R., Westerhoff, H.V. and van Niekerk, D.D. (2015). Quantitative analysis of drug effects at the whole-body level: a case study for glucose metabolism in malaria patients. *Biochemical Society Transactions*, vol. 43, no. 6, pp. 1157–1163.
- Sorensen, J.T. (1985). *A physiologic model of glucose metabolism in man and its use to design and assess improved insulin therapies for diabetes*. Ph.D. thesis, Massachusetts Institute of Technology.
- Srivastava, I.K., Schmidt, M., Grall, M., Certa, U., Garcia, A.M. and Perrin, L.H. (1992). Identification and purification of glucose phosphate isomerase of *Plasmodium falciparum*. *Molecular and Biochemical Parasitology*, vol. 54, no. 2, pp. 153–164.
- Sturm, A., Amino, R., Van de Sand, C., Regen, T., Retzlaff, S., Rennenberg, A., Krueger, A., Pollok, J.-M., Menard, R. and Heussler, V.T. (2006). Manipulation of host hepatocytes by the malaria parasite for delivery into liver sinusoids. *Science*, vol. 313, no. 5791, pp. 1287–1290.
- Teusink, B., Passarge, J., Reijenga, C.A., Esgalhado, E., van der Weijden, C.C., Schepper, M., Walsh, M.C., Bakker, B.M., van Dam, K., Westerhoff, H.V. *et al.* (2000). Can yeast glycolysis be understood in terms of in vitro kinetics of the constituent enzymes? Testing biochemistry. *European Journal of Biochemistry*, vol. 267, no. 17, pp. 5313–5329.
- Tsutsu, N., Takata, Y., Nunoi, K., Kikuchi, M., Takishita, S., Sadoshima, S. and Fujishima, M. (1989). Glucose tolerance and insulin secretion in conscious and unrestrained normotensive and spontaneously hypertensive rats. *Metabolism*, vol. 38, no. 1, pp. 63–66.

- Van Dooren, G.G., Stimmler, L.M. and McFadden, G.I. (2006). Metabolic maps and functions of the *Plasmodium mitochondrion*. *FEMS Microbiology Reviews*, vol. 30, no. 4, pp. 596–630.
- Vander Jagt, D.L., Hunsaker, L.A. and Heidrich, J.E. (1981). Partial purification and characterization of lactate dehydrogenase from *Plasmodium falciparum*. *Molecular and Biochemical Parasitology*, vol. 4, no. 5, pp. 255–264.
- Wernsdorfer, W.H. and Payne, D. (1991). The dynamics of drug resistance in *Plasmodium falciparum*. *Pharmacology & Therapeutics*, vol. 50, no. 1, pp. 95–121.
- Winzeler, E.A. (2008). Malaria research in the post-genomic era. *Nature*, vol. 455, no. 7214, pp. 751–756.
- Wiser, M.F. and Schweiger, H.-G. (1985). Cytosolic protein kinase activity associated with the maturation of the malaria parasite *Plasmodium berghei*. *Molecular and biochemical parasitology*, vol. 17, no. 2, pp. 179–189.
- Wongsrichanalai, C., Pickard, A.L., Wernsdorfer, W.H. and Meshnick, S.R. (2002). Epidemiology of drug-resistant malaria. *The Lancet Infectious Diseases*, vol. 2, no. 4, pp. 209–218.
- Wunderlich, J., Rohrbach, P. and Dalton, J.P. (2012). The malaria digestive vacuole. *Front Biosci*, vol. 4, pp. 1424–1448.
- Younis, Y., Chibale, K., Douelle, F., Cabrera, D.G., Feng, T.-S., Le Manach, C., Nchinda, A.T., Paquet, T., Street, L.J., Gordon, R. *et al.* (2014). Antimalarial 2-aminopyridine mmv390048 clinical candidate: Discovery and target identification studies. In: *Abstracts of Papers of the American Chemical Society*, vol. 248.